TECHNICAL REPORT R-104

LOCAL HEAT TRANSFER AND RECOVERY TEMPERATURES ON A YAWED CYLINDER AT A MACH NUMBER OF 4.15 AND HIGH REYNOLDS NUMBERS

By IVAN E. BECKWITH and JAMES J. GALLAGHER

Langley Research Center
Langley Air Force Base, Va.

TECHNICAL REPORT R-104

LOCAL HEAT TRANSFER AND RECOVERY TEMPERATURES ON A YAWED CYLINDER AT A MACH NUMBER OF 4.15 AND HIGH REYNOLDS NUMBERS [1]

By Ivan E. Beckwith and James J. Gallagher

SUMMARY

Local heat transfer, equilibrium temperatures, and wall static pressures have been measured on a circular cylinder at yaw angles of 0°, 10°, 20°, 40°, and 60°. The Reynolds number range of the tests was from 1×10^6 to 4×10^6 based on cylinder diameter.

Increasing the yaw angle from 0° to 40° increased the stagnation-line heat-transfer coefficients by 100 to 180 percent. A further increase in yaw angle to 60° caused a 40-percent decrease in stagnation-line heat-transfer coefficients.

At zero yaw angle the boundary layer over the entire front half of the cylinder was laminar but at yaw angles of 40° and 60° it was evidently completely turbulent, including the stagnation line, as determined by comparison of local heat-transfer coefficients with theoretical predictions. The level of heating rates and the nature of the chordwise distribution of heat transfer indicated that a flow mechanism different from the conventional transitional boundary layer may have existed at the intermediate yaw angles of 10° and 20°. At all yaw angles the peak heat-transfer coefficient occurred at the stagnation line and the chordwise distribution of heat-transfer coefficient decreased monotonically from this peak.

The average heat-transfer coefficients over the front half of the cylinder are in agreement with previous data for a comparable Reynolds number range.

The theoretical heat-transfer distributions for both laminar and turbulent boundary layers are calculated directly from simple quadrature formulas derived in the present report.

INTRODUCTION

Design studies of hypersonic lifting vehicles have generally indicated that aerodynamic heating may be reduced by using highly swept configurations with blunted leading edges. For laminar boundary layers the effect of sweep angle Λ on the heat transfer at the leading edge is usually taken as $\cos\Lambda$ as shown by the data of Feller (ref. 1) who measured the average heat transfer on the front half of a swept cylinder. More recent data (refs. 2 and 3) have indicated that the effect of sweep may be more nearly $\cos^{3/2}\Lambda$ which, at a sweep angle of 75°, would result in a 50-percent reduction of the heat transfer predicted by the $\cos\Lambda$ variation. The data and theory of reference 4 also indicate a $\cos^{3/2}\Lambda$ variation but the theories of references 5 and 6 indicate a variation somewhere between $\cos\Lambda$ and $\cos^{3/2}\Lambda$ for large stream Mach numbers.

The data of reference 7, in contrast to the investigations just cited, showed large increases in average heat transfer to a circular leading edge with increasing Λ up to a Λ of about 40°. These increases in heat transfer were probably caused by transition to turbulent flow which apparently resulted primarily from the inherent instability of the three-dimensional boundary-layer flow on a yawed cylinder. The leading-edge Reynolds numbers of reference 7 were considerably larger than the values in references 1 to 4 and were also larger than typical values for full-scale leading edges of hypersonic vehicles; hence, the main application of the high Reynolds number tests will probably be to bodies at angle of attack.

[1] Supersedes declassified NASA Memorandum 2-27-59L by Ivan E. Beckwith and James J. Gallagher, 1959.

In reference 8 it was shown that, even for bodies of moderate fineness ratio at angles of attack of about 20° or more, the heat transfer in a turbulent boundary layer is nearly the same as that for a turbulent boundary layer on a comparable yawed cylinder of large aspect ratio. The laminar theory of reference 9 predicts essentially the same result; that is, the heat transfer on a slender cone at an angle of attack of about 15° is already the same as that on a corresponding infinite cylinder at 75° yaw or sweep.

The present investigation was undertaken in an attempt to understand better and to explain the results of reference 7 by means of local measurements of heat transfer to a circular cylinder. The tests were conducted at a stream Mach number of 4.15 and a stream Reynolds number range of 1×10^6 to 4×10^6 based on cylinder diameter. The experimental results are compared with theories for local heat transfer in both laminar and turbulent boundary layers on yawed infinite cylinders. The laminar theory is based on the similar solutions of reference 10 for arbitrary pressure gradient. The turbulent theory makes use of the integral momentum and energy equations, simplified by means of Stewartson's transformation (ref. 11), together with suitable assumptions for velocity and thermal profiles, skin friction, and Reynolds analogy.

SYMBOLS

a constant coefficient in skin-friction law (see eq. (3))

a_o stagnation speed of sound

C constant in equation (B10)

c_p specific heat at constant pressure

D cylinder diameter

E integral thickness parameter, $\int_0^{\delta_Y} \frac{U}{U_1}\left(1-\frac{V}{V_1}\right)dZ$

G integral thickness parameter, $\int_0^{\delta_Y}\left[1-\left(\frac{V}{V_1}\right)^2\right]dZ$

H stagnation enthalpy, $c_pT+\frac{u^2+v^2}{2}$

h heat-transfer coefficient, $\frac{q_w}{T_{aw}-T_w}$

$\overline{h}$ heat-transfer parameter, $\frac{T_o-T_w}{T_{aw}-T_w}\theta'_w$

k thermal conductivity

l reference length

M Mach number

n reciprocal of exponent in skin-friction law (see eq. (3))

N_{Pr} Prandtl number (0.7 used in all calculations except as noted), $\frac{c_p\mu}{k}$

p pressure

Q resultant velocity in transformed coordinate system, $\sqrt{U^2+V^2}$

q local heat-transfer rate per unit area

$\overline{q}$ heat transfer in transformed coordinate system defined by equation (A5)

R Reynolds number based on diameter, $\frac{\rho u_R D}{\mu}$

r recovery factor

T temperature

$t=\frac{T}{T_o}$

U chordwise velocity in transformed coordinate system (see eq. (A4))

u chordwise velocity

u_R resultant velocity

V spanwise velocity in transformed coordinate system (see eq. (A4))

v spanwise velocity

X chordwise coordinate (transformed system; see eq. (A4))

x chordwise coordinate (normal to cylinder axis; physical boundary-layer system)

Z coordinate normal to surface (transformed system; see eq. (A4))

z coordinate normal to surface (physical boundary-layer system)

α angle between local streamline and cylinder axis

β pressure gradient parameter (see eq. (B11))

γ ratio of specific heats (1.40 used in all calculations)

Δ thermal boundary-layer thickness

δ velocity boundary-layer thickness in transformed coordinate system

δ^* integral thickness parameter, $\int_0^{\delta_X}\left(1-\left(\frac{U}{U_1}\right)\right)dZ$

η similarity variable

θ^* angular distance around cylinder from stagnation line in a plane normal to cylinder axis

θ enthalpy profile parameter, $\frac{H-H_w}{H_1-H_w}$

$\overline{\theta}$ integral thickness parameter, $\int_0^{\delta_X}\left[\frac{U}{U_1}-\left(\frac{U}{U_1}\right)^2\right]dZ$

Θ integral thickness parameter, $\int_0^{\Delta}\frac{U}{U_1}(1-\theta)dZ$

Θ^* integral thickness parameter, $\int_0^{\Delta}(1-\theta)dZ$

Λ yaw angle (complement of acute angle between free-stream flow direction and cylinder axis)

μ viscosity coefficient

ν coefficient of kinematic viscosity, μ/ρ

ρ density

τ shear at wall

$\overline{\tau}$ shear in transformed coordinate system defined by equation (A5)

Subscripts:

av average

aw zero heat transfer at wall over entire surface

e local equilibrium wall conditions (vanishing local heat transfer)

L laminar

N component normal to cylinder axis

o free-stream stagnation conditions

p external surface of heat-meter plug

r reference point within boundary layer

R resultant

s value at stagnation line (when used on a gas property such as ρ, T, etc., denotes that the property is evaluated outside the boundary layer at stagnation line)

T turbulent

t stagnation conditions downstream of normal shock

w wall conditions

X chordwise

Y spanwise

∞ free-stream conditions ahead of bow shock

1 local conditions just outside boundary layer

A prime denotes differentiation with respect to η.

APPARATUS

TUNNEL

The tests were conducted in one of the blowdown tunnels of the Gas Dynamics Branch at the Langley Research Center. The tunnel is a conventional two-dimensional nozzle with a test section 12 inches wide and 13 inches high. The nominal Mach number in the test section is 4.15 ± 0.03. The stagnation temperature for these tests ranged between 150° F and 300° F. Further details of tunnel operation and flow calibration may be found in references 7 and 12.

MODELS AND INSTRUMENTATION

Two different models were used in this investigation. The models were circular cylinders made from stainless steel and were the same in all respects except for the type of steel used and the dimensional details of the heat-sensitive elements or heat meters, which were similar to those described in reference 12. A sketch showing the location of the heat meters (designated as stations 1, 2, and 3) and including pertinent dimensions applying to both models is presented in figure 1(a). For all the configurations tested, end plates similar to that illustrated for the cylinder at 40° yaw in figure 1(a) were used on the models. The distances that the end plates extended ahead of the models for all yaw angles are given in the figure. The width of the end plates was held constant for all yaw angles.

The first model was constructed of type 304 stainless steel, and water was used as the coolant. This model had to be discarded after several tests at 40° yaw angle had been completed because of erratic data obtained as a result of the corrosive action of the water on the electrical leads and heat meters. Subsequently, a second model was constructed in which an improved heat-meter design was used. The coolant used in this model was Varsol (hydrocarbon solvent, boiling point 150° F to 200° F), which is both noncorrosive and nonconducting and may be cooled to a lower temperature than water. The second model was used for the remainder of the tests at yaw angles of 0°, 10°, 20°,

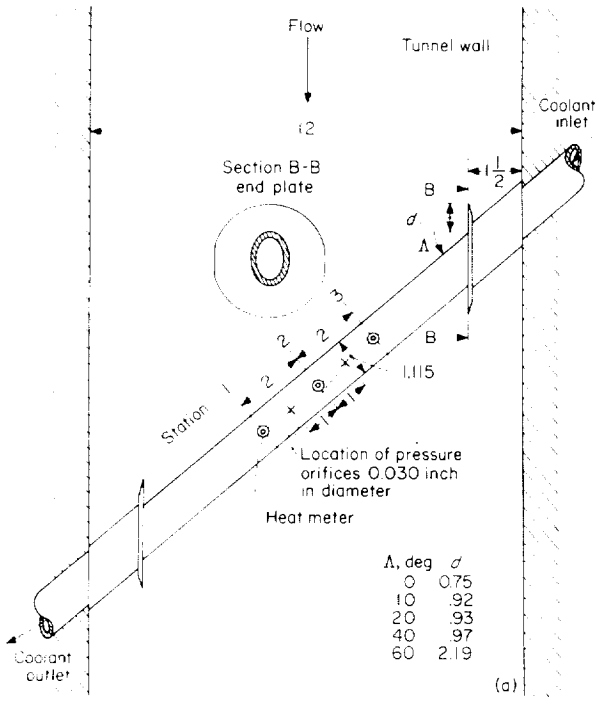

(a) Model installation.

FIGURE 1. Schematic diagram of apparatus. All dimensions are in inches.

and 60°. The heat meters used in the second model will be described in some detail.

A sectional sketch of the heat meter is shown in figure 1(b). The principle of operation of the heat meter is described in detail in reference 12. Briefly, the two interfaces at the stainless-steel and constantan joints are the hot and cold junctions of a thermocouple circuit. The thermoelectric output is then proportional to the quantity

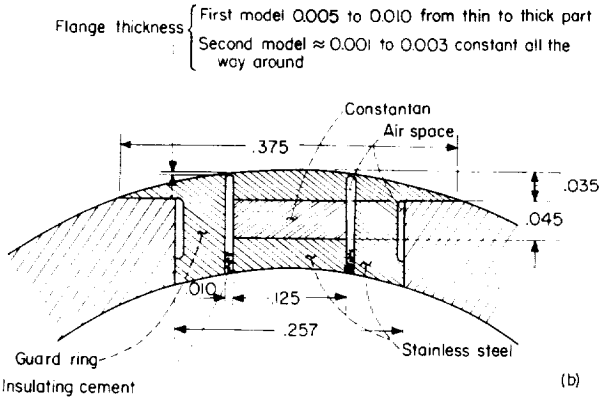

(b) Enlarged cross-sectional sketch of heat meter used in second model.

FIGURE 1. Continued.

of heat flowing through the constantan disk when steady temperatures are attained. A guard ring, as shown in figure 1(b), was used to reduce heat-conduction errors. Type 416 stainless steel was used for the second model and heat-meter parts because the thermal conductivity of this steel is approximately equal to that of constantan with the result that the meters and model wall are more nearly homogeneous. Careful measurements were made of each of the components so that after the units were soldered together the thickness of the flanges and copper-constantan joints would be known. For these heat meters the total thickness of the joints is less than 0.0005 inch. In reference 12 it is shown that the correction for heat conduction in the flanges depends critically on the flange thickness, which, for these meters, was 0.001 to 0.003 inch. The heat meters used in the first model were similar to those just described except for the flange thickness, which was about 0.008 inch, and the thermal conductivity of the 304 stainless steel (approximately three-fourths of the value for constantan).

Although extreme care was used in the construction of the heat meters it was found that the voltage outputs of all three meters were not the same under similar heating conditions. A calibrator, a sketch of which is shown in figure 1(c), was then made. It consisted of a copper-constantan heat meter with two guard rings and with one end contoured to fit the model. The second ring of the calibrator was also a heat meter so that the heat flux through it could be measured. The outside of the calibrator was insulated. Copper was used to insure a uniform temperature distribution in the unit. The upper end of the calibrator was heated electrically. A 0.0005-inch plastic film was used between the calibrator and the model during calibration to insulate it electrically from the model. The calibrator was centered over a heat meter and a constant coolant flow rate through the model was established. After steady temperatures were obtained, the heat flux through the calibrator could be calculated from the voltage output and the known conductivity and thickness of the constantan in the calibrator. Since the diameter of the center portion of the calibrator was the same as the heat-meter diameter (0.125 inch) and since the heat flux through the second ring of the calibrator was in all cases approximately equal to the heat flux through the center,

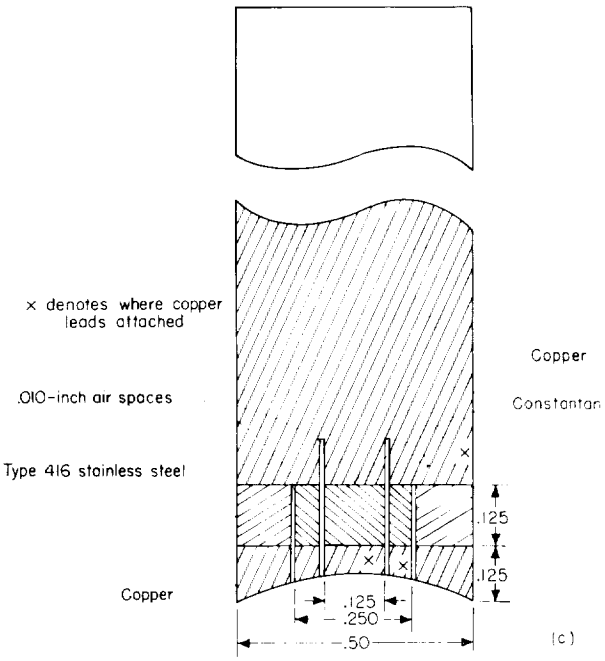

(c) Enlarged cross section of heat-meter calibrator.

FIGURE 1. Concluded.

it was assumed that this latter value was the correct heat flow into the meter. (Note that when the calibrator is properly centered over the heat meter, there is no heat flow into the outer surface of the heat-meter flange.) The ratio of this calculated heat-flow rate through the center of the calibrator to the indicated value from the heat meter in the model was then used as a correction factor to apply to all test data. The factors for the heat meters in the second model were 1.22, 0.95, and 1.01 at stations 1, 2, and 3, respectively.

Chromel-alumel thermocouples were used to measure the inside surface temperatures. The leads were spotwelded side by side at the inside surface of the heat meters.

The electrical output of the heat meters was amplified by a direct-current amplifier and fed into a self-balancing potentiometer. The output of the thermocouples was fed directly into a self-balancing potentiometer. A similar instrument was used to record stream stagnation temperature. The stagnation pressure was measured with a Bourdon pressure gage. The pressure distributions on the models were measured on mercury manometers whenever possible. Gages were used for pressures exceeding 60 pounds per square inch gage. The locations of the pressure orifices are shown in figure 1(a).

The model was rotated 180° during the tests by means of an actuator and pulleys so that a complete chordwise survey of the heat transfer and pressure distribution around the cylinder could be made during a single test. The surveys or distributions were thus obtained in planes normal to the cylinder axis. The temperature of the coolant was adjusted by pumping it through either a cooler (alcohol and dry-ice heat exchanger) or a heater (steam heat exchanger) or any combination of each. The temperature of the Varsol could be varied from −50° F to 150° F and the water temperature from 60° F to 200° F.

TEST METHODS AND DATA REDUCTION

The tests were conducted in the following manner. The tunnel and piping system were first preheated to the desired stagnation temperature. The model was polished; then the temperature of the coolant was adjusted and steady airflow was established.

Two series of runs were made at each yaw angle. The first series was made at approximately constant tunnel conditions and the heat rates were changed by changing the model temperature (varying the coolant temperature). The results from a typical set of runs at three coolant temperatures are shown in figure 2 where a heating-rate parameter $\frac{q_w D}{k_\infty T_o R_\infty}$ is plotted against a wall temperature parameter $\frac{T_o - T_p}{T_o}$. As pointed out

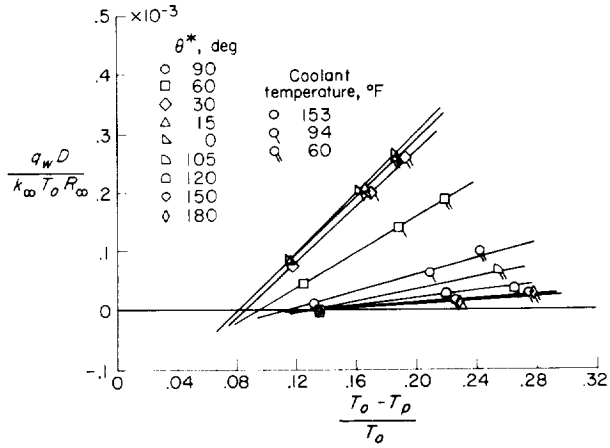

FIGURE 2. Variation of heat-transfer parameter with wall-temperature parameter at station 2 for typical runs. $\Lambda = 60°$; $T_o \approx 250°$ F; $R_\infty \approx 1.4 \times 10^6$.

in reference 12, the slope of these lines is proportional to the heat-transfer coefficient and the recovery temperature may be obtained from the intercept on the abscissa. Sufficient runs of this type were made so that the variation of T_r/T_o with Reynolds number was obtained. Then the second series of runs was made to obtain the variation of hD/k_∞ with Reynolds number. This was done by varying the stagnation pressure which ranged from 230 to 500 pounds per square inch gage.

All data presented in the report have been corrected by using the calibration constants previously discussed. A flange-conduction correction, which is described in detail in the appendix of reference 12, has also been applied to all data. This correction was taken to be a constant (0.7) for all the meters and is believed to be correct to within ± 10 percent according to calculations made by the method of reference 12, which uses measured heat rates and calculated plug temperatures. The plug temperature T_p is the outside surface temperature calculated from the measured inside surface temperature and the assumption of one-dimensional heat flow through the plug.

Radiation has been neglected since for all cases the radiation is very small compared with the aerodynamic heat transfer.

RESULTS AND DISCUSSION

PRESSURE DISTRIBUTIONS

Pressure-distribution data are presented because they are required in the theoretical heat-transfer calculations and also to provide a comparison with similar data from other investigations (for example, refs. 13 and 14) where test conditions and model end supports or configurations are generally different. The present data are plotted in figure 3 as the ratio of p_1/p_s against θ^* for $\Lambda = 0°$, 20°, 40°, and 60°. Also shown in figure 3 are curves

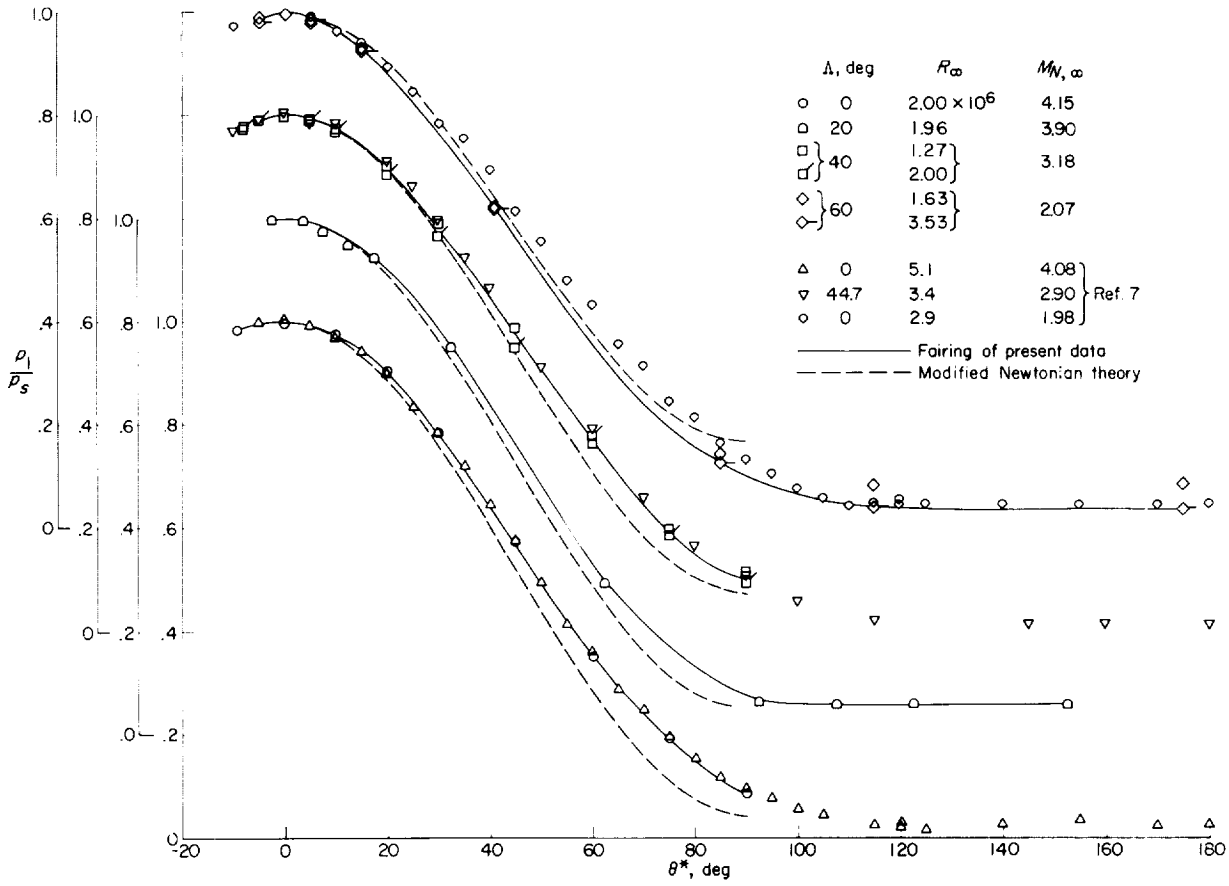

FIGURE 3.—Pressure distributions on circular cylinder.

calculated from modified Newtonian theory which predicts the pressure distribution

$$\frac{p_1}{p_s}=\left(1-\frac{p_\infty}{p_s}\right)\cos^2\theta^*+\frac{p_\infty}{p_s} \tag{1}$$

where p_∞/p_s depends only on the normal Mach number component. The experimental values of p_1/p_s, however, are seen to be essentially independent of the normal Mach number or yaw angle and would all fall approximately on one curve in agreement with the data of reference 13 as shown in reference 4.

The pressure data from reference 7 have been converted to p_1/p_s and are plotted in figure 3. At comparable yaw angles and normal Mach numbers the data are in good agreement except at $\Lambda=60°$ and $M_{N,\infty}=2.07$. Thus, even though the normal Mach numbers are about the same (2.07 in the present data and 1.98 in ref. 7) the pressures on the yawed cylinder in the present investigation are less than those on the unyawed cylinder of reference 7 up to about $\theta^*=100°$. The trend appears to be the same as that shown in the data of reference 4 where the pressures increase as the normal Mach number decreases. This condition indicates that at the larger yaw angles the pressure distribution on a yawed cylinder is not solely a function of the normal Mach number.

Spanwise (parallel to cylinder axis) variations in pressure were small and apparently were caused by variations in tunnel flow which are shown in the tunnel calibration data of reference 7.

The effect of Reynolds number on the pressure distribution is also small except on the back of the cylinder in the separated flow region where the pressure ratio decreases with increasing R_∞.

HEAT TRANSFER AND RECOVERY TEMPERATURES

Comparison of data and theory at stagnation line.—The values of the Nusselt number from station 2 at the stagnation line of the cylinder are plotted against stream Reynolds number in figure 4 for $\Lambda=0°$, 10°, 20°, 40°, and 60°. The lines shown in the figure are the corresponding theoretical values calculated for laminar and turbulent boundary layers.

The equation used to calculate the values shown in figure 4 for heat transfer in a turbulent boundary layer at the stagnation line of the

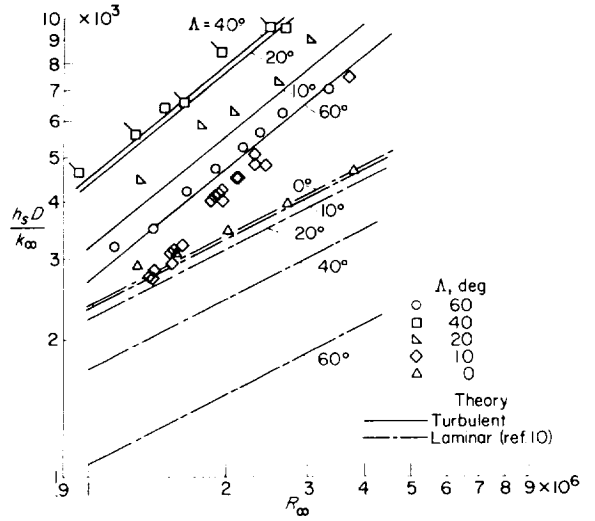

FIGURE 4.—Nusselt number at the stagnation line, spanwise station 2. Tailed symbols indicate data from first model.

cylinder is written

$$\frac{h_s D}{k_\infty}=\left(\frac{u_{R,\infty}D}{\nu_\infty}\right)^{\frac{n}{n+1}} N_{Pr}^{1/3}\left(a\frac{\mu_w}{\mu_o}\frac{T_\infty}{T_w}\frac{p_s}{p_\infty}\right)^{\frac{n}{n+1}}(\sin\Lambda)^{\frac{n-1}{n+1}}$$
$$\left[\frac{49}{376}\frac{\mu_o}{\mu_\infty}\cos\Lambda\left(\frac{D}{u_\infty}\frac{du_1}{dx}\right)_s\right]^{\frac{1}{n+1}} \tag{2}$$

where a and n are constants in the Blasius skin-friction law

$$\frac{\bar{\tau}}{\rho_o Q_1^2}=a\left(\frac{\nu_o}{Q_1\delta}\right)^{1/n} \tag{3}$$

For the present calculations these values were taken as $a=0.0228$ and $n=4$. Equation (2) predicts zero heat transfer at $\Lambda=0°$ and a peak in stagnation-line heat transfer at $\Lambda\approx30°$ followed by a decrease in heat transfer of about 40 percent from $\Lambda=40°$ to 60°. The predicted zero heat transfer at the stagnation line for zero yaw angle is not physically realistic since presumably a laminar boundary layer would always exist for these conditions with no possible mechanism present to cause a turbulent boundary layer. The complete derivation of equation (2) is given in appendix A. Briefly, the integral momentum and energy equations for the turbulent boundary layer on a yawed infinite cylinder are solved by using simplifying assumptions for skin friction, velocity and thermal profiles, secondary flow, and Reynolds analogy. Probably the most

restrictive assumptions in this analysis are: (1) The flat-plat skin-friction law in the form of equation (3) applies at any point on the cylinder as determined by local boundary-layer thickness and local resultant flow direction; (2) zero secondary flow exists over the entire cylinder (correct at $\Lambda=0$ and at stagnation line only for $\Lambda>0$); (3) and the flat-plate Reynolds analogy applies between the heat transfer and resultant shear.

The equation used to calculate the theoretical laminar heat-transfer values shown in figure 4 is

$$\frac{h_s D}{k_\infty}=0.773\left(\frac{R_\infty}{M_\infty}\frac{\mu_s}{\mu_\infty}\right)^{1/2}\left[\frac{T_\infty}{T_s}\frac{p_s}{p_\infty}\left(\frac{p_s}{p_\infty}-1\right)\right]^{1/4} \quad (4)$$

which is derived in appendix B and applies only for $N_{Pr}=0.7$ and $M_{N,\infty}>1.5$. Equation (4) is based on the exact solutions of reference 10 for the laminar compressible boundary layer on yawed infinite cylinders. The principal assumptions used in reference 10 are constant specific heats, constant Prandtl number, and the perfect gas law. The variation of heat-transfer coefficient with yaw angle as predicted by equation (4) can be closely approximated by $(\cos\Lambda)^{1.1}$ for large stream Mach numbers. (See appendix B.)

At a yaw angle of 0° the data are in good agreement with laminar theory except at the lowest Reynolds number where the data are about 8 percent higher than the theoretical values. At a yaw angle of 10° the data are in agreement with values obtained by laminar theory at the lowest Reynolds number but, as the Reynolds number is increased, the data become much higher than values indicated by laminar theory and tend to approach the line calculated by turbulent theory. The data at a yaw angle of 20° appear to vary as R_∞ to a constant power (straight-line variation) and are from about 75 to 130 percent higher than laminar-theory values and about 20 percent less than turbulent-theory values. At yaw angles of 40° and 60° the data are in good agreement with predictions from turbulent theory.

A possible explanation for the behavior of the data at yaw angles of 10° and 20° is as follows: Since the data at 0° yaw are in agreement with laminar-theory calculations and the data at 40° and 60° yaw are in agreement with the turbulent-theory calculations, it may be tentatively assumed that the theories are generally valid. Then, since the data at 10° and 20° yaw agree with neither theory, the boundary layer at these yaw angles (and R_∞ range of these tests) is in some transitional phase. The tendency of these data to approach a straight-line variation with R_∞ (in the log-log plot) over such a large range of R_∞ and Λ indicates that some flow mechanism different from the conventional transitional type of flow may be present. This different flow mechanism could be the vortical-type flow first observed by the British on swept wings (ref. 15) and also reported, for example, in reference 16. Another factor tending to indicate the existence of a flow mechanism (at yaw angles of 10° and 20°) different from the conventional transitional or turbulent boundary layer is that the heat transfer at the stagnation line was always the maximum value measured while the distribution of heat transfer around the cylinder decreased monotonically with increasing θ^* up to the separation line of the chordwise flow. This condition is in contrast to the situation on a blunt body of revolution where conventional transition to turbulent flow is generally marked by a sudden increase in local heat transfer as shown, for example, in reference 12.

The variation with yaw angle of $\frac{h_s D}{k_\infty}$ and $\left(\frac{T_e}{T_o}\right)_s$ is shown in figure 5. The heat-transfer data are a cross plot of figure 4 at values of R_∞ of 1.3×10^6, 2.0×10^6, and 3.5×10^6. The recovery-temperature data are obtained from plots similar to figure 2 at $R_\infty\approx1.3\times10^6$. The large increases in heat transfer with increasing yaw angle up to 40° are clearly apparent in figure 5. It may be noted again that at yaw angles of 10° and 20° the heat-transfer coefficients are below turbulent theory but at yaw angles of 40° and 60° good agreement between data and theory is obtained. The recovery temperatures decrease with increasing yaw angle as predicted by both laminar and turbulent theory according to the equation

$$\left(\frac{T_e}{T_o}\right)_s=r\left(1-\frac{T_s}{T_o}\right)+\frac{T_s}{T_o} \quad (5)$$

where the recovery factor r was taken as $N_{Pr}^{1/2}$ for laminar boundary layers (see refs. 6 and 10) and $N_{Pr}^{1/3}$ for turbulent boundary layers. Although the recovery-temperature ratios are less than the theoretical values, the variation with Λ

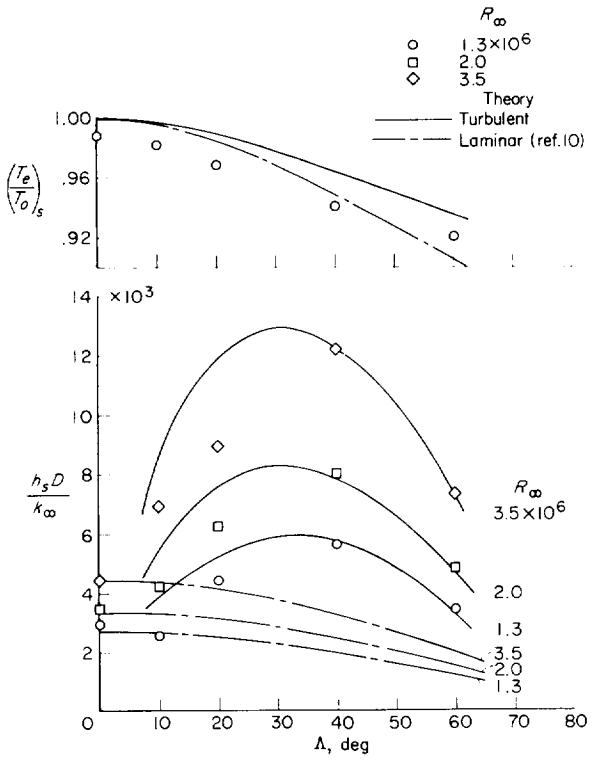

FIGURE 5.—Variation of recovery temperature and Nusselt number with yaw angle Λ at the stagnation line of the cylinder from station 2.

from Λ=20° to 60° tends to parallel the theoretical turbulent variation. The effect of R_∞ on the recovery temperatures was generally less than 1 percent which is considered to be within the range of experimental errors.

An indication of how well the ideal of an infinite cylinder was realized can be obtained from figure 6 where the spanwise variations of $\frac{h_s D}{k_\infty}$ are shown for Λ=0°, 10°, 20°, 40°, and 60° at $R_\infty=1.3\times10^6$, 2×10^6, and 3.5×10^6. The data are cross plots obtained from $\frac{h_s D}{k_\infty}$ plotted against R_∞ for each spanwise station. These spanwise stations were located 2 inches apart along a generating element of the cylinder as shown in the sketch of figure 1(a). Figure 6 shows that the spanwise variations are within the expected experimental error of ±10 percent except at Λ=10° and $R_\infty=1.3\times10^6$. The reason for the increase in spanwise variations for these conditions is probably that transition has just been initiated at approximately these values of Λ and R_∞ as discussed in connection with figure 4.

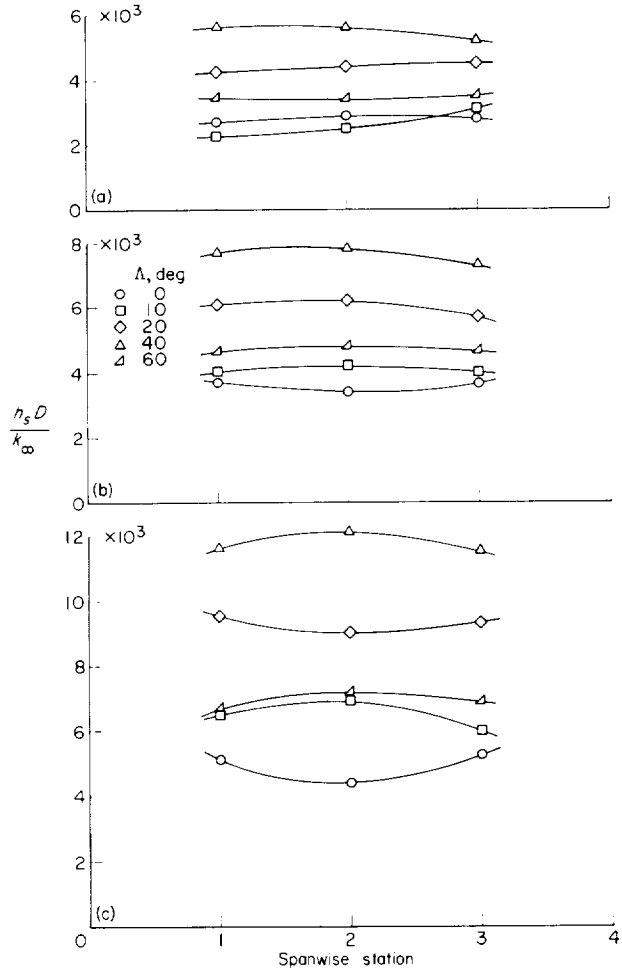

(a) $R_\infty=1.3\times10^6$.
(b) $R_\infty=2.0\times10^6$.
(c) $R_\infty=3.5\times10^6$.

FIGURE 6.—Spanwise variation of Nusselt number at stagnation line of cylinder.

Hence, it can be concluded that, within the experimental accuracy, the heat-transfer data are representative of conditions on an infinite cylinder.

The effect of interference from the end plates on the bow shock is shown in figure 7 in which two schlieren photographs of the cylinder at a yaw angle of 60° are presented. The flow direction in these photographs is from left to right and planform views of the cylinder and bow shock are shown. In figure 7(a) a portion of the upstream end plate is visible in the upper left-hand corner of the figure. A disturbance which apparently originates at the leading edge of the end plate is seen to

intersect the bow shock. However, the effect of this disturbance is negligible at the center portion of the cylinder since, as shown in figure 7(b), the bow shock is essentially parallel to the cylinder in this region.

Circumferential distribution of heat transfer and recovery temperatures and comparison with theory.—The experimental values of Nusselt number $\frac{hD}{k_\infty}$ at station 2 on the model are plotted against the circumferential angle θ^* in figure 8 for $\Lambda=0°$, 10°, 20°, 40°, and 60° for several values of R_∞. All data have been corrected for the calibration constant and heat loss by conduction through the heat-meter flange as discussed previously.

Also shown in figures 8(a) to 8(e) are the theoretical distributions of $\frac{hD}{k_\infty}$ for corresponding values of R_∞ as computed for laminar and turbulent boundary layers by the approximate methods discussed in appendixes A and B. Both the laminar and turbulent values of $\frac{hD}{k_\infty}$ were calculated from the equation

$$\frac{hD}{k_\infty}=\frac{h_sD}{k_\infty}\frac{h}{h_s} \tag{6}$$

where for the laminar boundary layer (appendix B)

$$\left(\frac{h}{h_s}\right)_L=\left(\frac{p_1}{p_s}\right)^{8/7}\left[\frac{\frac{dU'_1}{dX'}U'_1X'}{2\left(\frac{dU'_1}{dX'}\right)_s}\right]^{1/2}\frac{\theta'_w}{(\theta'_w)_{\beta=1}} \tag{7}$$

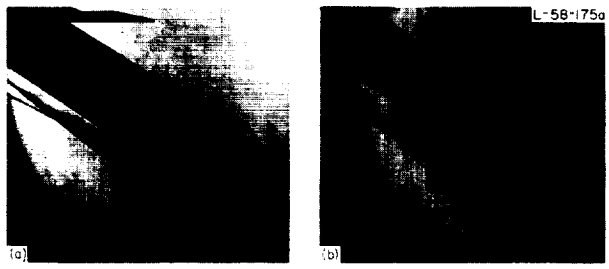

(a) Flow in vicinity of upstream end plate.

(b) Flow in vicinity of station 2.

FIGURE 7.—Schlieren photographs of model at 60° yaw. Optical distortion in schlieren system causes apparent slight taper in model. $R_\infty\approx1.5\times10^6$.

and for the turbulent boundary layer (appendix A)

$$\left(\frac{h}{h_s}\right)_T=\left(\frac{p_1}{p_s}\right)^{8/7}\left[\frac{\left(\frac{p_s}{p_1}\right)^{2/7}-\frac{T_s}{T_o}}{1-\frac{T_s}{T_o}}\right]^{\frac{n}{2n}\frac{1}{1}}\left(\frac{\delta_s}{\delta}\right)^{1/n} \tag{8}$$

where the wall temperature is assumed to be constant. The values of $\frac{h_sD}{k_\infty}$ in equation (6) were obtained from equations (2) or (4). As shown in the appendixes, the only information needed to evaluate equations (7) and (8) is the pressure distribution around the cylinder (experimental pressure distributions were used in all cases except at $\Lambda=10°$), stream Mach number and stagnation conditions, yaw angle, and wall temperature. For the laminar case the ratios $\theta'_w/(\theta'_w)_{\beta=1}$ from reference 10 for $N_{Pr}=1.0$ are given in table I. The calculations for all values of Λ were not extended beyond $\theta^*\approx100°$ since flow separation presumably occurred near this value of θ^* as indicated by the approximately constant value of p_1/p_s for $\theta^*>100°$ in the pressure data of figure 3.

For a yaw angle of 0° (fig. 8(a)), the data are seen to be in good agreement with laminar theory over the entire forward section of the cylinder. The data (particularly for the largest Reynolds number) tend to be somewhat higher than the laminar theory for $\theta^*\geqq60°$. These higher values may be caused by the nonisothermal wall temperatures during the tests. Both the laminar and turbulent calculations from equations (7) and (8) are for an isothermal wall. The curves for turbulent theory at $\Lambda=0°$ shown in figure 8(a) were calculated directly from equations (A11) and (A12) and are included for comparative purposes.

The data at a yaw angle of 10° (fig. 8(b)) are in agreement with laminar theory at the lowest Reynolds number; however, for the larger value of R_∞ the data are considerably higher than the values predicted by laminar theory and up to about $\theta^*=60°$ are still not so high as the values predicted by turbulent theory. (Both Newtonian pressure distribution and experimental p_1/p_s from $\Lambda=0°$ were used for the theoretical calculations at $\Lambda=10°$ since experimental pressures were not available.) If the boundary layer at these larger values of R_∞ were of the conventional transition

TABLE I. RATIO OF HEAT-TRANSFER COEFFICIENTS

[From ref. 10; $N_{Pr}=1.0$; linear viscosity relation; zero transpiration cooling]

$\frac{1}{t_s}$	β	$\frac{\theta'_w}{(\theta'_w)_{\beta=1}}$ for values of t_w of—		
		0	0.5	1.0
1.0	2.0	1.0274	1.0489	1.0608
	1.5	1.0158	1.0282	1.0352
	1.0	1.0000	1.0000	1.0000
	.5	.9753	.9565	.9448
	.2	.9514	.9153	.8885
	0	.9268	.8663	.8231
1.6	2.0	1.0373	1.0602	1.0720
	1.5	1.0217	1.0349	1.0420
	1.0	1.0000	1.0000	1.0000
	.5	.9661	.9445	.9327
	.2	.9320	.8872	.8612
	0	.8948	.8198	.7706
3.0	2.0	1.0514	1.0747	1.0849
	1.5	1.0302	1.0438	1.0498
	1.0	1.0000	1.0000	1.0000
	.5	.9509	.9288	.9180
	.2	.8993	.8509	.8261
	0	.8381	.7478	.6936
6.5	2.0	1.0684	1.0891	1.0972
	1.5	1.0404	1.0525	1.0574
	1.0	1.0000	1.0000	1.0000
	.5	.9319	.9118	.9034
	.2	.8553	.8103	.7904
	0	.7509	.6510	.5966

type, an increase in heat transfer denoting transition to a completely turbulent boundary layer might be expected at some location downstream of the stagnation line. Since this increase did not occur in the present tests, it may be inferred that a different flow mechanism is present such as the streamwise vortical flow observed, for example, in references 15 and 16. A flow of this nature might be expected to cause heat-transfer rates intermediate between the rates for a laminar and completely turbulent boundary layer and also would be expected to extend forward to the vicinity of the stagnation line at sufficiently large Reynolds numbers. (See ref. 15.) Transition to completely turbulent flow has apparently not occurred (at least for $75°>\theta^*>0$) at $\Lambda=10°$ and

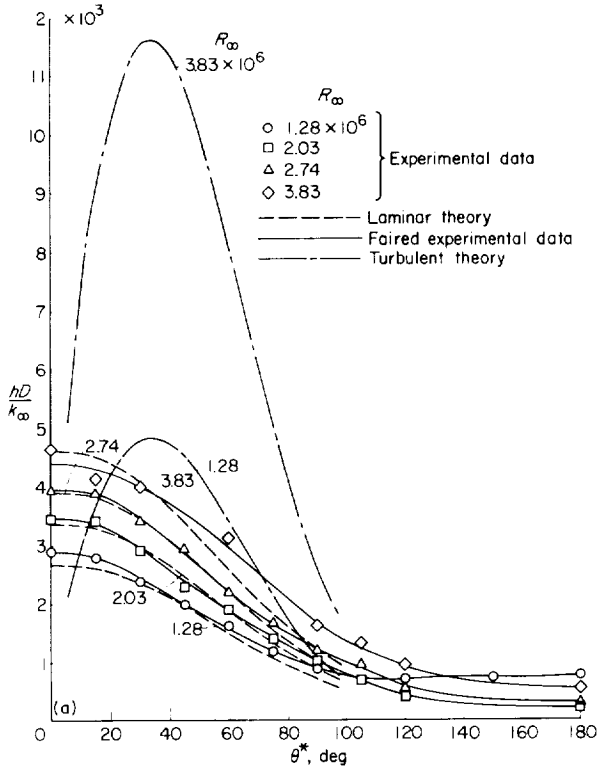

(a) $\Lambda=0°$.

FIGURE 8. Variation of Nusselt number around circumference of cylinder at station 2.

$R_\infty \leqq 3.8\times10^6$, not only because the experimental values are below theoretical turbulent values but also because no peak in heat-transfer rates was observed as is predicted by the theory for small values of Λ. A peak in the heat-transfer distribution is to be expected in a turbulent boundary layer on cylinders at small yaw angles by analogy with the corresponding theoretical predictions for an unyawed cylinder or a body of revolution as shown, for example, in reference 12.

At $\Lambda=20°$ (fig. 8(c)), the experimental data are well above the theoretical laminar values and below the theoretical turbulent values except for $\theta^*>60°$. Here again it may be speculated that a flow mechanism different from the conventional transitional type may exist since no increase in heat transfer occurred with increasing θ^* around the cylinder. The fact that the data for both $\Lambda=10°$ and 20° are higher than theoretical turbulent values for large values of θ^* is probably an indication of errors in the theory rather than

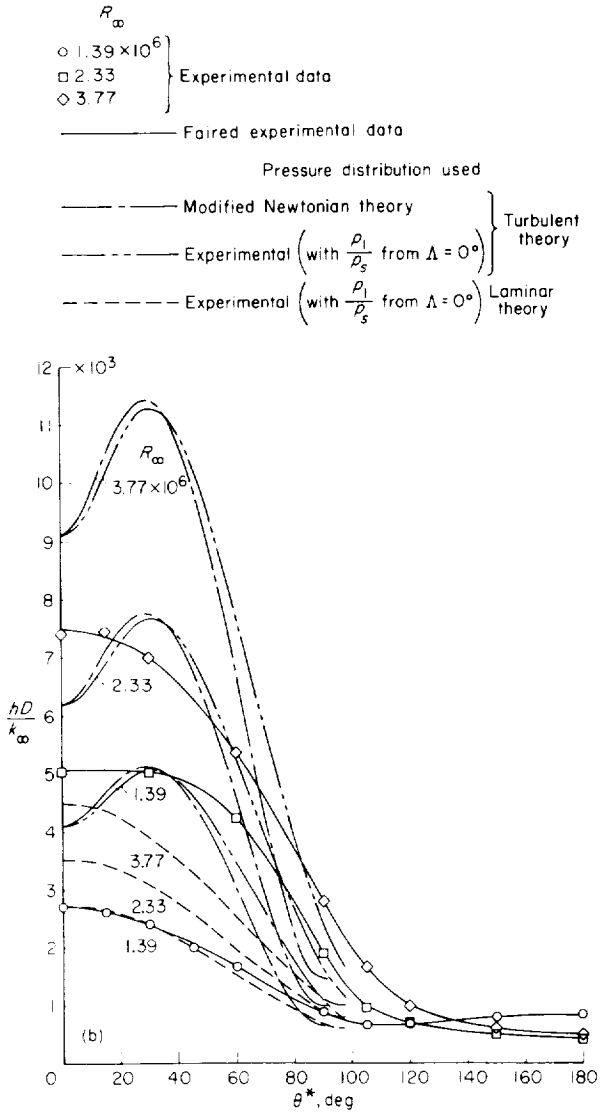

(b) $\Lambda = 10°$.

FIGURE 8.—Continued.

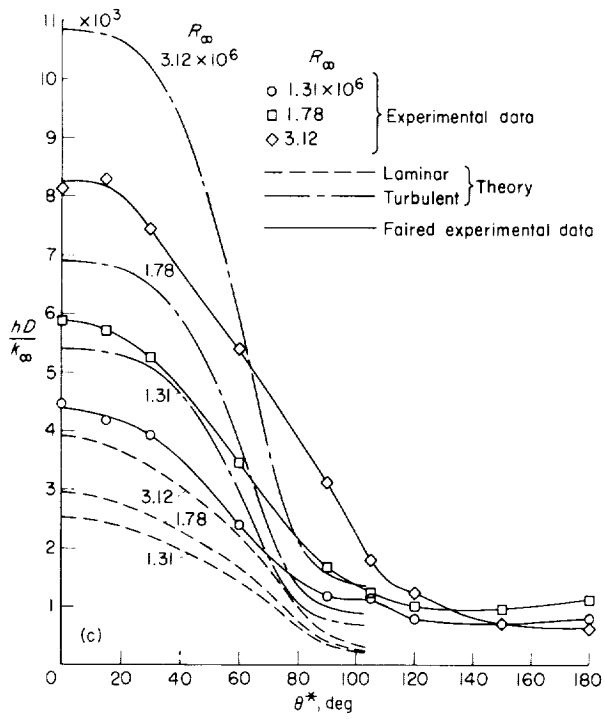

(c) $\Lambda = 20°$.

FIGURE 8.—Continued.

the possible development of a turbulent boundary layer on the cylinder. That is, the errors caused by the simplifying assumptions, such as zero secondary flow, isothermal wall, and flat-plate skin friction are expected to increase with increasing distance from the stagnation line. (See appendix A.)

In contrast to the results at $\Lambda = 10°$ and 20°, the data at $\Lambda = 40°$ (fig. 8(d)) are in fairly good agreement or are generally somewhat higher than the theoretical turbulent distributions over the entire forward region of attached flow. At $\Lambda = 60°$ (fig. 8(e)) the theory underestimates the heat-transfer coefficient for large values of θ^* by as much as 50 percent whereas at $\Lambda = 40°$ the agreement between data and theory is good except at $R_\infty = 1.49 \times 10^6$ and 2.75×10^6 with the second model. On the basis of this comparison, the boundary layer is probably completely turbulent (including the flow at the stagnation line) for yaw angles of about 40° or greater. The larger discrepancy between theory and data from the second model at $\Lambda = 40°$ is believed to be caused by differences in heat-meter construction as discussed in the section entitled "Apparatus." The data from the second model are believed to be more nearly correct.

Downstream from the separation line, which from figure 3 is in the vicinity of $\theta^* = 110°$, the heat-transfer coefficients for all values of Λ are approximately constant. The values of the heat-transfer coefficients in this separated-flow region are from about 10 to 15 percent of the stagnation-line value except at $\Lambda = 0°$ and 10° with $R_\infty < 2 \times 10^6$.

Experimental and theoretical values of the ratio

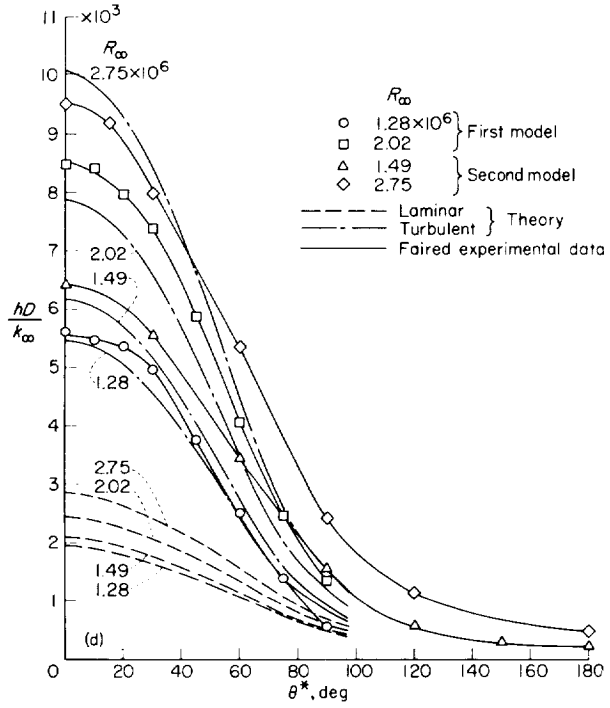

(d) $\Lambda=40°$.

FIGURE 8.—Continued.

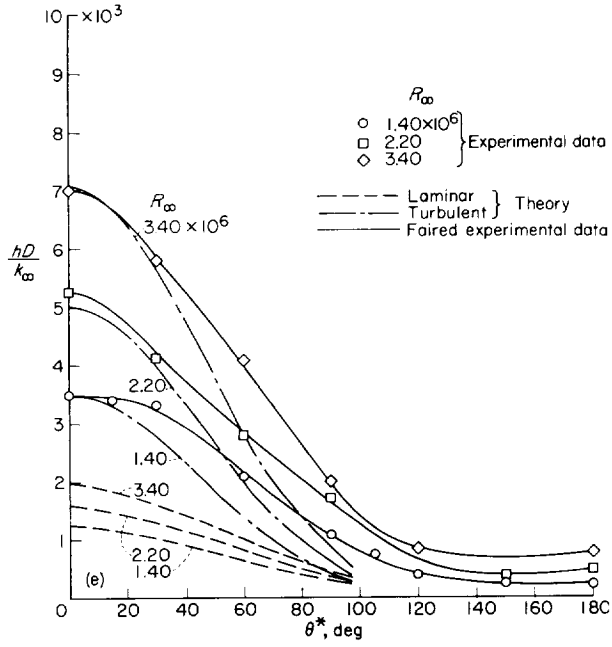

(e) $\Lambda=60°$.

FIGURE 8.—Concluded.

of local recovery temperature to stagnation temperature T_e/T_o are shown in figure 9. The experimental data were obtained from plots similar to figure 2 and the theoretical values were calculated from equation (5) after replacing T_s/T_o with T_1/T_o. Experimental values of p_1/p_s were used to evaluate T_1/T_o except for $\Lambda=10°$ where the pressure ratio distribution for $\Lambda=0°$ was used. Over the front half of the cylinder the recovery-temperature data are always below those for the turbulent theory (figs. 9(a) to 9(e)), and at $\Lambda=0°$, 10°, and 40°, the data are also somewhat below the laminar theory but at $\Lambda=20°$ the data tend to approach the turbulent theory for $\theta^*>60°$. At $\Lambda=60°$ (fig. 9(e)), the data are between the curves for the laminar and turbulent theory. In general, then, no definite indications as to which type of flow is present can be obtained from the recovery-temperature data; however, the small

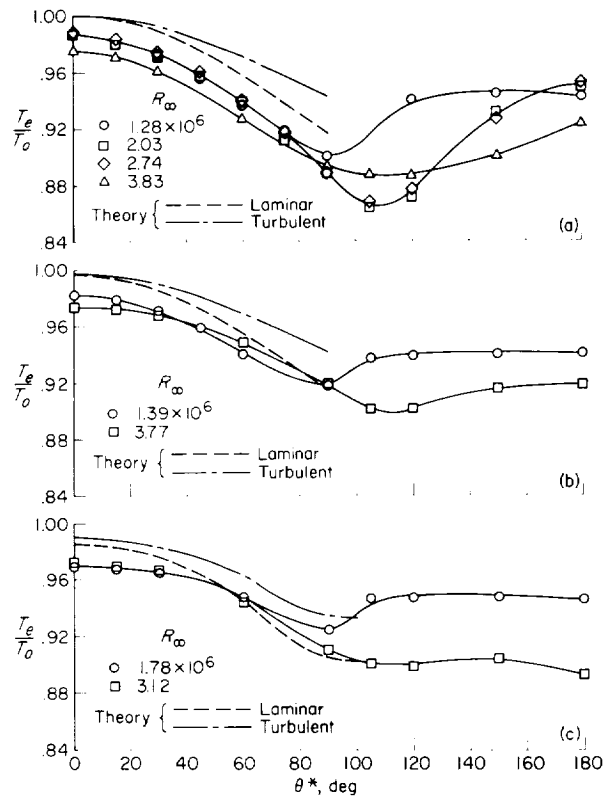

(a) $\Lambda=0°$.
(b) $\Lambda=10°$.
(c) $\Lambda=20°$.

FIGURE 9.—Variation of recovery temperature around circumference of cylinder at station 2.

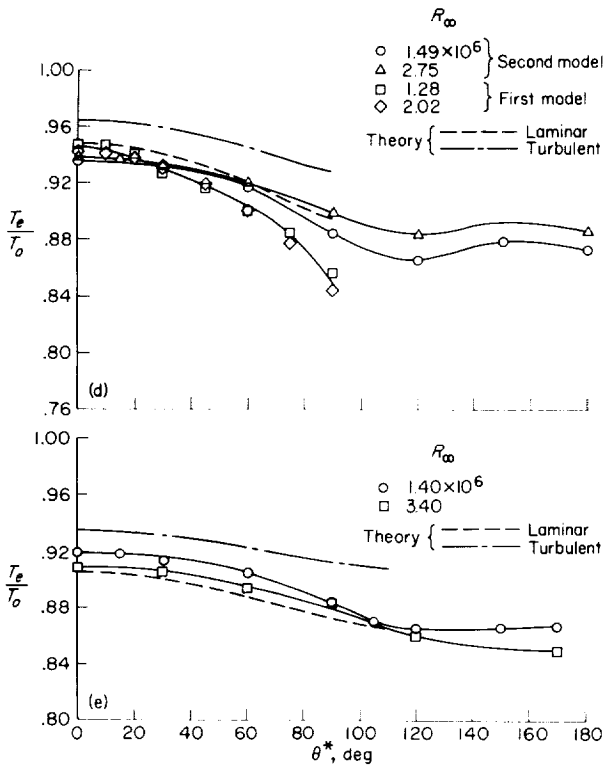

(d) $\Lambda = 40°$.
(e) $\Lambda = 60°$.

FIGURE 9.—Concluded.

differences involved are probably within the experimental error.

At $\Lambda = 40°$ (fig. 9(d)) the values of T_e/T_o for the first model are smaller for $\theta^* > 30°$ than the values from the second model. This discrepancy is again presumably caused by differences in heat-meter construction.

Effect of chordwise temperature gradient. The differences in the heat transfer and recovery temperature distributions between the first and second models at $\Lambda = 40°$ as shown in figures 8(d) and 9(d) may have been caused partly by the different chordwise wall-temperature distributions for the two models. (Chordwise is here used in the sense of describing the circumferential distribution in a plane normal to the cylinder axis.) These wall temperature distributions are different because of the different coolants used, water in the first model and Varsol in the second model. An attempt was made to evaluate this effect of wall temperature gradients from an additional set of tests with the second model using water as a coolant instead of Varsol.

In figure 10 the ratio T_p/T_o is plotted against θ^* for typical runs with the second model for which water and Varsol were used as coolants. Since water is a more efficient coolant, the temperature distribution for the water-cooled model is more nearly isothermal than that for the Varsol cooled model, and hence the chordwise temperature gradients are smaller for the water-cooled model.

Also shown in the upper part of figure 10 are the ratios of equilibrium to stagnation temperatures that were obtained by using the two coolants. A qualitative analysis of the effect of upstream temperature distributions such as those of figure 10 on local equilibrium temperature (wall temperature required for zero heat transfer) indicates that, as the temperature distribution becomes more nearly isothermal, the local equilibrium temperature would decrease. This result is in agreement with the present data since the water-cooled model was always more nearly isothermal than the Varsol cooled model.

It can also be shown that the local heat rate would be smaller when the upstream temperature distribution is more nearly isothermal if the local temperature potential (difference between recovery and wall temperature) is held constant.

The effect of wall temperature gradients on the Nusselt number or heat-transfer coefficient is determined by the relative changes in both the heat rates and temperature potential. Nusselt number distributions from the tests on the second

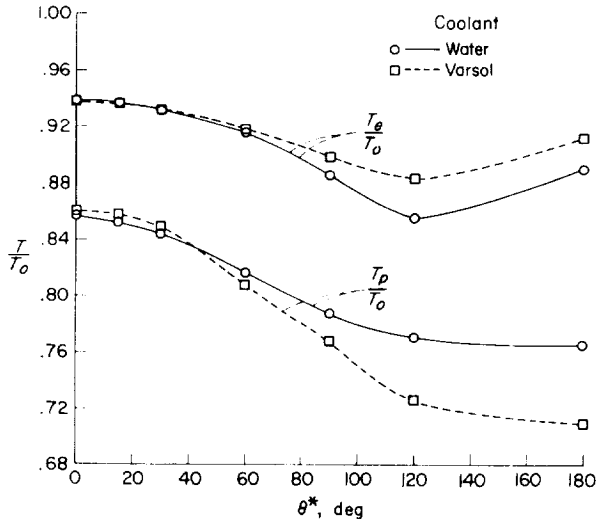

FIGURE 10.—Effect of coolant on temperature distributions for $\Lambda = 40°$ and $R_\infty = 2.75 \times 10^6$. (Data from station 1 on the second model.)

model with water and Varsol used as coolants are shown in figure 11. Comparison of these data indicates that the heat-transfer coefficient decreases more with increasing θ^* on the water-cooled model.

The data of figure 10 were used to calculate the effect of wall temperature gradients in a turbulent boundary layer by the method of reference 17. This method is based on an approximate solution of the integral energy equation for the incompressible turbulent boundary layer on a flat plate with a stepwise temperature distribution at the surface of the plate. The method is extended approximately to the case of a pressure gradient by using the difference $T_p - T_e$ rather than T_p as the dependent variable. The results of the calculation for the temperature distributions of figure 10 indicated that at $\theta^*=90°$ the heat-transfer coefficient on the Varsol cooled model would be about 11 percent larger than the value on the water-cooled model. This value compares with a value of 20 percent from the data of figure 11.

This discussion indicates that the differences in the data as shown in figure 11 may be partly caused by the different wall temperature gradients. However, the effects are within the experimental accuracy so that no definite conclusion is possible except that the larger differences between the data from the first and second models are not caused entirely by wall temperature gradients. It should be noted that, although local heat-transfer coefficients at large values of θ^* may be influenced by temperature-gradient effects, the average or total heat transfer to the cylinder would be changed at most by only a few percent since most of the total heat is transferred at small values of θ^*.

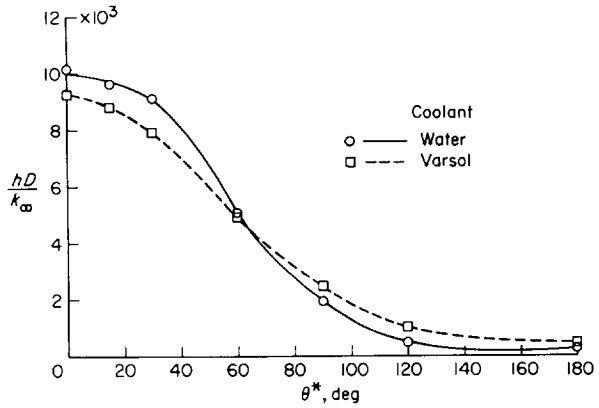

FIGURE 11.—Effect of coolant on Nusselt number distribution at station 1 on second model. $\Lambda=40°$; $R_\infty=2.75\times10^6$.

Average heat transfer over front half of cylinder.—The average Nusselt number over the forward portion of the cylinder from $\theta^*=0°$ to 90° was obtained by integration of plots similar to figure 8. The results have been plotted against R_∞ in figure 12. Also plotted in the figure for comparison are data from reference 7 where the average heat transfer to the front half of a ½-inch-diameter copper cylinder was measured directly. At comparable yaw angles the two sets of data are seen to be in good agreement. Since the small copper model of reference 7 presumably had essentially an isothermal wall temperature distribution, this good agreement indicates that the wall temperature variations encountered in the present tests had very little effect on the average heat-transfer coefficients. The reason for this small effect can be seen from figure 11 which shows that different wall temperature gradients such as those of figure 10 could not have any significant effect on the average heat-transfer coefficient over the front half of the cylinder. It therefore seems reasonable that the average heat-transfer coefficients for an isothermal model would be about the same as the present results within the experimental error.

Also shown in figure 12 are the average heat-transfer coefficients from the turbulent and laminar theories of the present report as discussed in appendixes A and B. At $\Lambda=0°$ the data are in good agreement with laminar theory but at $\Lambda=10°$ and 20° (fig. 12(a)) the data increase with increasing Reynolds number and tend to approach the turbulent theory. Note that these average data are generally in better agreement with the corresponding theoretical results than the stagnation-line data of figure 4. The reason for this better agreement is apparent from the distributions shown in figures 8(b) and 8(c). At $\Lambda=40°$ (fig. 12(b)) the data are in good agreement with turbulent theory. At $\Lambda=60°$ the data are about 15 percent higher than the present theoretical values but are in good agreement with the theoretical values of reference 7. This latter theory is based on an average flat-plate correlation formula using a reference temperature and the cross-flow velocity for a yawed cylinder. The value of an empirical constant was obtained from the data of reference 7. The agreement between the present

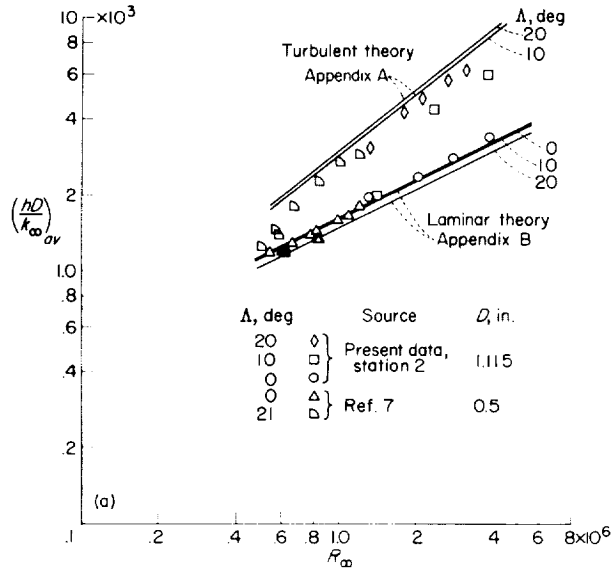

(a) Λ=0°, 10°, and 20°.

FIGURE 12. Average Nusselt number on front half of circular cylinder.

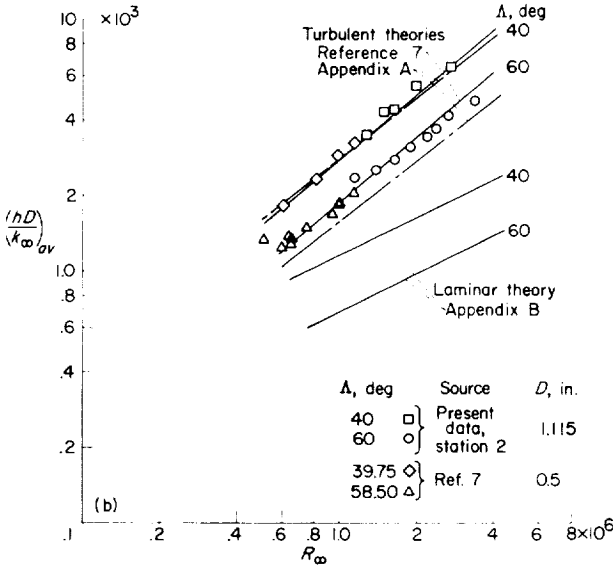

(b) Λ=40° and 60°.

FIGURE 12.— Concluded.

data and the data of reference 7 indicates that this same constant also applies to the present data. The present theory for a turbulent boundary layer (appendix A) is apparently in considerable error at large values of θ^* when Λ is also large, possibly because of the simplifying assumption of zero secondary flow which, for large values of θ^*, would tend to increase with increasing Λ. This error is also apparent in figure 8(e) which shows that the present theory underestimates the local heat transfer by 50 percent at $\theta^*=90°$ and Λ=60°.

CONCLUDING REMARKS

Local heat transfer, equilibrium temperatures, and wall static pressures have been measured on a circular cylinder at yaw angles of 0°, 10°, 20°, 40°, and 60°. The tests were made at a stream Mach number of 4.15 and stream Reynolds number range of 1×10^6 to 4×10^6 based on cylinder diameter.

The pressure distributions up to the separation line of the chordwise flow were essentially independent of normal Mach number and yaw angle Λ.

At the stagnation line of the cylinder the heat-transfer coefficients increased from 100 to 180 percent, depending on the Reynolds number, as the yaw angle was increased from 0° to 40°. Increasing the yaw angle from 40° to 60° resulted in a 40-percent decrease in heat-transfer coefficients. At zero yaw the data are in agreement with theory for laminar boundary layers and at 40° and 60° yaw the data agree with a theory for turbulent boundary layers. At yaw angles of 10° and 20° the data were generally somewhere between the theoretical laminar and turbulent values.

The chordwise distribution of heat-transfer coefficients up to the separation line was in good agreement with laminar theory at zero yaw angle. At yaw angles of 10° and 20° the chordwise distributions were generally above laminar theory and below turbulent theory. At any given yaw angle the heat transfer at the stagnation line was the peak value and the chordwise distribution always decreased monotonically from this peak value. The values of the heat-transfer coefficients as well as the chordwise distributions at yaw angles of 10° and 20° indicated that a boundary-layer flow mechanism different from the conventional transitional or turbulent flow may have been present. At yaw angles of 40° and 60° the chordwise distributions were in good agreement with turbulent theory except for large values of θ^* (angular distance from the stagnation line) at Λ=60°. On the downstream side of the cylinder in the separated-flow region where the theories do not apply, the heat-transfer coefficients were approximately constant at about 10 to 15 percent of the stagnation-line value.

The average heat-transfer coefficients over the front half of the cylinder are in agreement with previous data for a comparable Reynolds number range.

The theoretical heat-transfer distributions for both laminar and turbulent boundary layers are calculated directly from simple quadrature formulas derived in the appendixes. Simple formulas for calculating the stagnation-line heat transfer with both laminar and turbulent boundary layers are also presented. The theoretical variation of stagnation-line heat-transfer coefficient with yaw angle Λ is approximately $(\cos \Lambda)^{1.1}$ for laminar boundary layers but for turbulent boundary layers the heat-transfer coefficient increases at first, reaches a maximum at $\Lambda \approx 30°$, and then decreases about 40 percent from $\Lambda = 40°$ to 60°.

LANGLEY RESEARCH CENTER,
NATIONAL AERONAUTICS AND SPACE ADMINISTRATION,
LANGLEY AIR FORCE BASE, VA., *December 2, 1958.*

APPENDIX A

TURBULENT BOUNDARY-LAYER THEORY ON YAWED INFINITE CYLINDERS

The starting point of the present analysis is the integral equations of momentum and energy in the compressible boundary layer on a yawed infinite cylinder. These equations may be obtained directly from appendix B of reference 10 by replacing the expressions for laminar shear and heat transfer with general expressions which include the effects of turbulent shear and heat transfer. In terms of a modified Stewartson coordinate system and for zero normal velocity at the wall, these equations become

$$\frac{d\bar{\theta}}{dX}+\frac{1}{U_1}\frac{dU_1}{dX}\left[2\bar{\theta}+\delta^*+\left(\frac{T_o}{T_s}-1\right)G+\frac{T_o}{T_s}(t_w-1)\Theta^*\right]=\frac{\bar{\tau}_X}{\rho_o U_1^2} \tag{A1}$$

$$\frac{dE}{dX}+\frac{E}{U_1}\frac{dU_1}{dX}=\frac{\bar{\tau}_Y}{\rho_o U_1 V_1} \tag{A2}$$

$$\frac{d\Theta}{dX}+\Theta\left(\frac{1}{U_1}\frac{dU_1}{dX}+\frac{1}{t_w-1}\frac{dt_w}{dX}\right)=\frac{\bar{q}_w}{\rho_o U_1 c_p(T_o-T_w)} \tag{A3}$$

The transformed coordinates and velocities are related to the corresponding physical quantities by the following equations:

$$\left.\begin{aligned} X&=\int_0^x\frac{\mu_r\rho_r}{\mu_o\rho_o}\sqrt{\frac{\overline{T_1}}{T_o}}\,dx\\ Z&=\sqrt{\frac{\overline{T_1}}{T_o}}\int_0^z\frac{\rho}{\rho_o}\,dz\\ U&=\sqrt{\frac{T_o}{T_1}}\,u\\ V&=\sqrt{\frac{T_o}{T_1}}\,v\\ V_1&=\sqrt{\frac{T_o}{T_1}}\,u_{R,\infty}\sin\Lambda \end{aligned}\right\} \tag{A4}$$

The shear and heat transfer in the transformed system are related to the corresponding physical quantities by the following definitions:

$$\left.\begin{aligned} \bar{\tau}&=\frac{\mu_o\rho_o}{\mu_r\rho_r}\frac{T_o}{T_1}\tau\\ \bar{q}_w&=\frac{\mu_o\rho_o}{\mu_r\rho_r}\sqrt{\frac{T_o}{T_1}}\,q_w \end{aligned}\right\} \tag{A5}$$

where the subscript r denotes quantities evaluated at some reference point within the boundary layer. Essentially, the same transformation as equations (A4) has been used in reference 18 where good correlation with experimental skin-friction data on insulated plates was obtained by taking the reference point in the local free stream. In reference 19 the transformation was used to calculate heat transfer in turbulent boundary layers on blunt bodies, and better agreement with experimental data was generally obtained by evaluating the reference quantities so that the flat-plate skin-friction relation of reference 20 was satisfied when the method was applied to this case.

In order to get a practical solution to this system of equations, several simplifying assumptions are made. The basic ideas of the "line-of-flow principle" as discussed in reference 21 are adopted in contradiction to the "independence principle" of reference 22. The data of reference 23, as well as the discussion of reference 21, indicate that the independence principle does not apply to the growth of a turbulent boundary layer on a yawed flat plate. In accordance with the line-of-flow principle, it is assumed that the local resultant shear is a function of the resultant velocity at the edge of the boundary layer and that this shear is related to the heat transfer by a Reynolds analogy. The effects of a chordwise pressure gradient are accounted for approximately by expressing the shear in terms of local boundary-layer thickness.

The effects of compressibility are accounted for by expressing the skin-friction law in the transformed system. The equation for the transformed skin friction is then assumed to be of the Blasius type and is written as

$$\bar{\tau}_R=\sqrt{\bar{\tau}_X{}^2+\bar{\tau}_Y{}^2}=\rho_o Q_1{}^2 a\left(\frac{\nu_o}{Q_1\delta}\right)^{1/n} \tag{A6}$$

where δ is the velocity boundary-layer thickness and $Q_1=\sqrt{U_1{}^2+V_1{}^2}$ is the local transformed resultant velocity at the edge of the boundary layer. The Colburn modification (ref. 24) of the Reynolds analogy, also expressed in the transformed system, is

$$\frac{\bar{q}_w}{c_p\rho_o Q_1(T_{aw}-T_w)}=\frac{1}{N_{Pr}{}^{2/3}}\frac{\bar{\tau}_R}{\rho_o Q_1{}^2} \tag{A7}$$

In general, a secondary flow would exist and its limiting direction α_w at the wall with respect to the cylinder axis is determined by the ratio of chordwise to spanwise shears as given by

$$\tan\alpha_w=\frac{\bar{\tau}_X}{\bar{\tau}_Y} \tag{A8}$$

The velocity profiles are now assumed to be

$$\left.\begin{aligned}\frac{U}{U_1}&=\left(\frac{Z}{\delta}\right)^{1/7}\\ \frac{V}{V_1}&=\left(\frac{Z}{\delta}\right)^{1/5}\end{aligned}\right\} \tag{A9}$$

so that, from the definition of E and the assumption that $\delta_X=\delta_Y$,

$$\frac{E}{\delta}=\frac{49}{376} \tag{A10}$$

Then, from equations (A6), (A8), and (A10), equation (A2) may be written as

$$\frac{d}{dX}(U_1\delta)=\frac{376}{49}a\left(\frac{\nu_o U_1}{Q_1}\right)^{1/n}\frac{Q_1{}^2}{V_1}\frac{\cos\alpha_w}{(\delta U_1)^{1/n}} \tag{A11}$$

which, for the required boundary condition of finite δ at $X=0$, integrates to

$$\delta^{\frac{1+n}{n}}=\frac{376}{49}a\frac{1+n}{U_1{}^{\frac{1+n}{n}}}\int_0^X\left(\frac{\nu_o U_1}{Q_1}\right)^{1/n}\frac{Q_1{}^2}{V_1}\cos\alpha_w dX \tag{A12}$$

From equations (A5), (A6), and (A7) the general expression for the heat-transfer coefficient is

$$h\equiv\frac{q_w}{T_{aw}-T_w}=\frac{a}{N_{Pr}{}^{2/3}}\left(\frac{\nu_o}{Q_1\delta}\right)^{1/n}c_p\rho_o Q_1\frac{\mu_r\rho_r}{\mu_o\rho_o}\sqrt{\frac{T_1}{T_o}} \tag{A13}$$

HEAT TRANSFER AT THE STAGNATION LINE

On a cylinder with a blunt leading edge $U_1\to 0$, $Q_1\to V_1$, and $\alpha_w\to 0$ as $X\to 0$; hence, from equation (A11), the expression for δ_s is

$$\delta_s{}^{\frac{1+n}{n}}=\frac{376}{49}a(\nu_o)^{1/n}\left(\frac{V_1{}^{\frac{n-1}{n}}}{\frac{dU_1}{dX}}\right)_{X=0} \tag{A14}$$

At the stagnation line, equation (A13) becomes

$$h_s=\frac{a}{N_{Pr}{}^{2/3}}\left(\frac{\nu_o}{\delta_s}\right)^{1/n}c_p\rho_o(V_1)^{\frac{n-1}{n}}\sqrt{\frac{T_s}{T_o}}\left(\frac{\mu_r\rho_r}{\mu_o\rho_o}\right)_s \tag{A15}$$

By substituting equation (A14) for δ_s with

$$(V_1)_{X=0}=\sqrt{\frac{T_o}{T_s}}u_{R,\infty}\sin\Lambda$$

$$\left(\frac{dU_1}{dX}\right)_{X=0}=\left(\frac{\mu_o\rho_o}{\mu_r\rho_r}\right)_s\frac{T_o}{T_s}\left(\frac{du_1}{dx}\right)_s$$

(from equations (A4)) equation (A15) may be written, after some rearranging, as

$$\frac{h_s l}{k_o}=N_{Pr}{}^{1/3}\left(\frac{u_{R,\infty}l}{\nu_o}\right)^{\frac{n}{1+n}}\left(a\frac{\mu_r\rho_r}{\mu_o\rho_o}\right)_s^{\frac{n}{1+n}}(\sin\Lambda)^{\frac{n-1}{n+1}}\left(\frac{49}{376}\cos\Lambda\frac{l}{u_\infty}\frac{du_1}{dx}\right)_s^{\frac{1}{1+n}} \tag{A16}$$

In terms of a stream Nusselt and Reynolds number, equation (A16) becomes

$$\frac{h_s l}{k_\infty}=N_{Pr}{}^{1/3}\left(\frac{u_{R,\infty}l}{\nu_\infty}\right)^{\frac{n}{1+n}}\left(a\frac{p_s}{p_\infty}\frac{\mu_r}{\mu_n}\frac{T_\infty}{T_r}\right)_s^{\frac{n}{1+n}}(\sin\Lambda)^{\frac{n-1}{n+1}}\left(\frac{49}{376}\frac{\mu_n}{\mu_\infty}\cos\Lambda\frac{l}{u_\infty}\frac{du_1}{dx}\right)_s^{\frac{1}{1+n}} \tag{A17}$$

for constant values of c_p and N_{Pr}. The reference quantities μ_r and T_r were evaluated at the wall temperature for comparison with the experimental data of the present report.

CHORDWISE DISTRIBUTION OF HEAT TRANSFER

According to equations (A13) and (A14) the chordwise distribution of heat-transfer coefficient would be

$$\frac{h}{h_s}=\left(\frac{\delta_s}{\delta}\right)^{1/n}\left(\frac{Q_1}{V_{1,s}}\right)^{\frac{n-1}{n}}\sqrt{\frac{T_1}{T_s}\frac{p_1}{p_s}\frac{\mu_r T_{r,s}}{\mu_{r,s}T_r}} \quad \text{(A18)}$$

If the flow at the edge of the boundary layer is isentropic, then the relation between temperature and pressure is

$$\frac{T_1}{T_s}=\left(\frac{p_1}{p_s}\right)^{\frac{\gamma-1}{\gamma}}$$

The adiabatic energy equation requires that

$$\frac{u_1^2+v_1^2}{a_o^2}=\frac{2}{\gamma-1}\left(1-\frac{T_1}{T_o}\right)$$

so that from the definitions of the transformed velocities

$$\frac{Q_1}{a_o}=\sqrt{\frac{2}{\gamma-1}\left(\frac{T_o}{T_1}-1\right)}$$

Hence,

$$\frac{Q_1}{V_{1,s}}\equiv\frac{Q_1}{Q_{1,s}}=\left(\frac{\frac{T_s}{T_1}-\frac{T_s}{T_o}}{1-\frac{T_s}{T_o}}\right)^{1/2}$$

and equation (A18) may be written as

$$\frac{h}{h_s}=\frac{\mu_r T_{r,s}}{\mu_{r,s}T_r}\left(\frac{p_1}{p_s}\right)^{\frac{3\gamma-1}{2\gamma}}\left[\frac{\left(\frac{p_s}{p_1}\right)^{\frac{\gamma-1}{\gamma}}-\frac{T_s}{T_o}}{1-\frac{T_s}{T_o}}\right]^{\frac{n-1}{2n}}\left(\frac{\delta_s}{\delta}\right)^{1/n} \quad \text{(A19)}$$

From equations (A12), (A14), and (A4), the ratio of boundary-layer thicknesses is

$$\left(\frac{\delta}{\delta_s}\right)^{1/n}=\left[\frac{1+n}{n}\frac{\sqrt{\frac{T_o}{T_s}}\left(\frac{du_1}{dx}\right)_s^{\frac{1}{1+n}}}{U_1^{\frac{1}{n}}}\int_0^x\frac{\mu_r T_{r,s}}{\mu_{r,s}T_r}U_1^{1/n}\left(\frac{Q_1}{V_{1,s}}\right)^{\frac{n-1}{n}}\left(\frac{p_1}{p_s}\right)^{\frac{3\gamma-1}{2\gamma}}\frac{\cos\alpha_w}{\cos\alpha_1}dx\right]^{\frac{1}{1+n}} \quad \text{(A20)}$$

where

$$\cos\alpha_1=\frac{V_1}{Q_1}$$

$$\frac{U_1}{a_o}=\sqrt{\frac{2}{\gamma-1}\left[\left(\frac{p_s}{p_1}\right)^{\frac{\gamma-1}{\gamma}}-1\right]}$$

$$\frac{V_1}{a_o}=\sqrt{\frac{2}{\gamma-1}\left(\frac{p_s}{p_1}\right)^{\frac{\gamma-1}{\gamma}}\left(\frac{T_o}{T_s}-1\right)}$$

The only quantity as yet unspecified in equation (A20) is α_w, the angle of the "wall streamline" with respect to the cylinder axis. This angle could be determined from the simultaneous solution of equations (A1), (A2), and (A3) by using the shear and heat-transfer assumptions of equations (A6) and (A7). Such a solution is difficult to justify in view of the lack of knowledge concerning turbulent boundary layers on yawed bodies. Rather, the simplifying assumption of zero secondary flow is introduced at this point. That is

$$\alpha_w=\alpha_1=\tan^{-1}\frac{U_1}{V_1} \quad \text{(A21)}$$

which is exactly correct on the stagnation line and is expected to be a good approximation in the vicinity of the stagnation line. The secondary flow affects the heat transfer only through the factor $\frac{\cos\alpha_w}{\cos\alpha_1}$ which, for $n=4$, enters equation (A19) to the 1/5 power. This small power indicates that the assumption of zero secondary flow may not have much effect on the heat-transfer calculation except at large values of N or near a separation line. Evaluating the reference quantities at the wall and assuming that the wall is isothermal then gives the form of h/h_s shown in the text as equation (8) where δ_s/δ is obtained from equation (A20) with $\frac{\cos\alpha_w}{\cos\alpha_1}=1$ and $\frac{\mu_r T_{r,s}}{\mu_{r,s}T_r}=1$.

From equations (A7), (A8), and (A21), the assumption of zero secondary flow results in the following analogy between heat transfer and spanwise shear

$$\frac{\bar{q}_w}{\bar{c}_p\rho_o V_1(T_{aw}-\bar{T}_w)}=\frac{1}{N_{Pr}^{2/3}}\frac{\bar{\tau}_Y}{\rho_o V_1^2}$$

or

$$\frac{\overline{\tau}_Y}{\frac{1}{2}\rho_o V_1^2}\frac{V_1 l}{\nu_o}=\frac{2}{N_{Pr}^{1/3}}\frac{\overline{q}_w l}{k_o(T_{aw}-T_w)}$$

This relation may be written in terms of physical shear, heat transfer, and velocities as

$$\frac{\tau_Y}{\frac{1}{2}\rho_o v_1^2}\frac{\rho_o v_1 l}{\mu_o}=\frac{2}{N_{Pr}^{1/3}}\frac{hl}{k_o} \tag{A22}$$

which is of the same form as the corresponding analogy between heat transfer and spanwise shear for the exact laminar solutions of reference 6. In terms of the chordwise shear, equation (A22) becomes the flat-plate Reynolds analogy

$$\frac{\tau_X}{\frac{1}{2}\rho_o u_1^2}\frac{\rho_o u_1 l}{\mu_o}=\frac{2}{N_{Pr}^{1/3}}\frac{hl}{k_o}$$

which indicates that for zero secondary flow the effects of chordwise pressure gradient on Reynolds analogy are neglected.

APPENDIX B

HEAT TRANSFER IN THE LAMINAR BOUNDARY LAYER ON YAWED INFINITE CYLINDERS

SIMPLIFIED SOLUTION AT THE STAGNATION LINE

The results of the exact solutions of reference 10 are used to calculate the heat transfer in a laminar boundary layer. The basic equation for the heat-transfer coefficient at the stagnation line of a yawed infinite cylinder is

$$h_s \equiv \left(\frac{q_w}{T_{aw}-T_w}\right)_s = k_w\sqrt{\frac{\rho_w}{\mu_w}\left(\frac{du_1}{dx}\right)_s}\,\bar{h} \qquad \text{(B1)}$$

where for $N_{Pr}=0.7$, $\bar{h}$ is given approximately by the correlating equation

$$\bar{h}=0.5\left(\frac{\rho_s\mu_s}{\rho_w\mu_w}\right)^{0.44} \qquad \text{(B2)}$$

A general expression for the stream Nusselt number is then

$$\frac{h_s l}{k_\infty}=0.5\sqrt{\frac{\rho_\infty u_{R,\infty} l}{\mu_\infty}\frac{k_w}{k_\infty}}\sqrt{\frac{\mu_\infty}{\mu_w}\frac{\rho_w}{\rho_\infty}}\cos\Lambda\left(\frac{l}{u_\infty}\frac{du_1}{dx}\right)_s^{1/2}\left(\frac{\rho_s\mu_s}{\rho_w\mu_w}\right)^{0.44}$$

which, for constant c_p and N_{Pr}, becomes

$$\frac{h_s D}{k_\infty}=0.5\sqrt{R_\infty}\left[\cos\Lambda\left(\frac{D}{u_\infty}\frac{du_1}{dx}\right)_s\right]^{1/2}\left(\frac{\mu_w T_s}{\mu_s T_w}\right)^{0.06}\left(\frac{\rho_s\mu_s}{\rho_\infty\mu_\infty}\right)^{1/2} \qquad \text{(B3)}$$

in terms of the diameter D.

The stagnation-line velocity gradient calculated from the modified Newtonian pressure gradient is

$$\left(\frac{D}{u_\infty}\frac{du_1}{dx}\right)_s=\frac{2}{u_\infty}\left[2\frac{p_s}{\rho_s}\left(1-\frac{p_\infty}{p_s}\right)\right]^{1/2}$$

which according to reference 6 is in good agreement with experimental data for $M_{N,\infty}>1.5$. For a perfect gas, this expression for the velocity gradient becomes

$$\left(\frac{D}{u_\infty}\frac{du_1}{dx}\right)_s=\frac{2}{M_{N,\infty}}\left[\frac{2}{\gamma}\frac{T_s}{T_\infty}\left(1-\frac{p_\infty}{p_s}\right)\right]^{1/2} \qquad \text{(B4)}$$

Substitution of equation (B4) into equation (B3) then results in the equation

$$\frac{h_s D}{k_\infty}=0.5\left(2\frac{R_\infty}{M_\infty}\frac{\mu_s}{\mu_\infty}\right)^{1/2}\left[\frac{2}{\gamma}\frac{T_\infty}{T_s}\frac{p_s}{p_\infty}\left(\frac{p_s}{p_\infty}-1\right)\right]^{1/4} \qquad \text{(B5)}$$

where it has been assumed that

$$\left(\frac{\mu_w T_s}{\mu_s T_w}\right)^{0.06}\approx 1$$

Because of the small value of the exponent, this assumption is correct to within 1 or 2 percent over a wide range of temperatures. Equation (B5) applies only for $N_{Pr}=0.7$ and $M_{N,\infty}>1.5$.

The effect of yaw angle on the heat-transfer coefficient is obtained from equation (B5) as

$$\frac{h_s}{(h_s)_{\Lambda=0}}=\sqrt{\frac{\mu_s}{\mu_o}}\left(\frac{T_o}{T_s}\frac{\frac{p_s}{p_\infty}-1}{\frac{p_t}{p_\infty}-1}\right)^{1/4} \qquad \text{(B6)}$$

which for a perfect gas and Sutherland's viscosity temperature law may be closely approximated by $(\cos\Lambda)^{1.1}$ for large free-stream Mach numbers. Equation (B6) shows that for given values of M_∞ and Λ the ratio $h_s/(h_s)_{\Lambda=0}$ increases with an increase in temperature level because of the increase in μ_s/μ_o. This increase indicates that the effect of yaw as measured in a wind tunnel may be somewhat different than that measured in flight. Thus, for $M_\infty=4.0$ and $\Lambda=60°$, $h_s/(h_s)_{\Lambda=0}$ is about 9 percent larger at $T_\infty=390°$ R than at $T_\infty=160°$ R. It is of interest to compare equation (B6) with the result of the approximate analysis of reference 4. Thus, if a linear viscosity-temperature relation is assumed and the restriction of large normal Mach number (a small yaw angle being implied) is imposed so that $\frac{p_s}{p_\infty}>>1$, then equation (B6) reduces to

$$\frac{h_s}{(h_s)_{\Lambda=0}}=\left(\frac{T_s}{T_o}\right)^{1/4}\left(\frac{p_s}{p_t}\right)^{1/2}$$

which is exactly the same as equation (11) of reference 4.

CHORDWISE VARIATION OF HEAT-TRANSFER COEFFICIENT

A general expression for the heat-transfer rate from reference 10 is

$$q_w=k_w(T_o-T_w)\sqrt{\frac{\overline{T}_1}{T_o}\frac{p_1}{p_o}\frac{T_o}{T_w}}\sqrt{\frac{1}{2\nu_o}\left(\frac{dU_1}{dX}+\frac{U_1}{X}\right)}\left(\frac{\partial\theta}{\partial\eta}\right)_w \tag{B7}$$

where η is a similarity variable which can be written as

$$\eta=\left[\frac{1}{2\nu_o}\left(\frac{dU_1}{dX}+\frac{U_1}{X}\right)\right]^{1/2}Z$$

The ratio of the local heat transfer to the value at the stagnation line for isentropic flow at the edge of the boundary layer is then

$$\frac{q_w}{q_{w,s}}=\frac{k_w}{k_{w,s}}\frac{T_{w,s}}{T_w}\frac{T_o-T_w}{T_o-T_{w,s}}\left(\frac{p_1}{p_s}\right)^{\frac{3\gamma-1}{2\gamma}}\left[\frac{\frac{dU_1}{dX}+\frac{U_1}{X}}{2\left(\frac{dU_1}{dX}\right)_s}\right]^{1/2}\frac{\left(\frac{\partial\theta}{\partial\eta}\right)_w}{\left(\frac{\partial\theta}{\partial\eta}\right)_{w,s}} \tag{B8}$$

where

$$\left.\begin{aligned}\theta&=\frac{H-H_w}{H_1-H_w}\\ U_1&=\sqrt{\frac{\overline{T}_o}{T_1}}u_1=a_o\left\{\frac{2}{\gamma-1}\left[\left(\frac{p_s}{p_1}\right)^{\frac{\gamma-1}{\gamma}}-1\right]\right\}^{1/2}\\ X&=\int_0^x\frac{\mu_w}{\mu_o}\frac{\rho_w}{\rho_o}\sqrt{\frac{\overline{T}_1}{T_o}}\,dx\\ Z&=\sqrt{\frac{\overline{T}_1}{T_o}}\int_0^z\frac{\rho}{\rho_o}\,dz\end{aligned}\right\} \tag{B9}$$

If it is assumed that θ is a function only of η, then the similar solutions of reference 10 may be used where θ has been calculated for various values of T_w/T_o, T_o/T_s, and β with $N_{Pr}=1$. The ratio T_o/T_s is a parameter that depends on yaw angle and Mach number and β is the velocity-gradient parameter defined by the velocity distribution for a similar flow as

$$U_1=CX^{\frac{\beta}{2-\beta}} \tag{B10}$$

Solving for β gives

$$\beta=\frac{2\frac{dU_1}{dX}}{\frac{U_1}{X}+\frac{dU_1}{dX}} \tag{B11}$$

The simplest way to evaluate β is to calculate U_1 and X from the required pressure-distribution data by means of equations (B9) and then substitute these values directly into equation (B11). (This procedure is analogous to that of ref. 25.) The values of U_1 used in the present calculations are shown plotted against X/D in figure 13 which also includes for comparison the values calculated from Newtonian pressure distribution. The heat-transfer coefficient distribution then follows from equation (B8) as

$$\frac{h}{h_s}=\frac{k_w}{k_{w,s}}\frac{T_{w,s}}{T_w}\left(\frac{p_1}{p_s}\right)^{\frac{3\gamma-1}{2\gamma}}\left[\frac{\frac{dU_1}{dX}+\frac{U_1}{X}}{2\left(\frac{dU_1}{dX}\right)_s}\right]^{1/2}\frac{\overline{h}}{\overline{h}_s}$$

where for the present calculation it is assumed that

$$\left(\frac{\overline{h}}{\overline{h}_s}\right)_{N_{Pr}\neq1.0}\approx\left(\frac{\overline{h}}{\overline{h}_s}\right)_{N_{Pr}=1.0}$$

Then, since for $N_{Pr}=1.0$, $T_{aw}=T_o$, the following equation may be written:

$$\left(\frac{\overline{h}}{\overline{h}_s}\right)_{N_{Pr}=1.0}=\left(\frac{\theta'_w}{\theta'_{w,s}}\right)_{N_{Pr}=1.0}=\left[\frac{\theta'_w}{(\theta'_w)_{\beta=1.0}}\right]_{N_{Pr}=1.0}$$

The quantity θ'_w is tabulated in reference 10 as a function of T_w/T_o, T_o/T_s, and β for $N_{Pr}=1$. Values of the ratio $\theta'_w/(\theta'_w)_{\beta=1}$ are given in table I in the present report.

An alternative procedure analogous to the method of reference 26 is one in which an "equivalent" wedge flow is found for each segment of the given velocity distribution. The value of β is found from the simultaneous solution of equation (B10) evaluated at the end points of each segment and the equation (from ref. 10)

$$\Theta=\left[(2-\beta)\nu_o\frac{X}{U_1}\right]^{1/2}\theta'_w$$

evaluated at the first point of the segment where X is now considered as the chordwise length

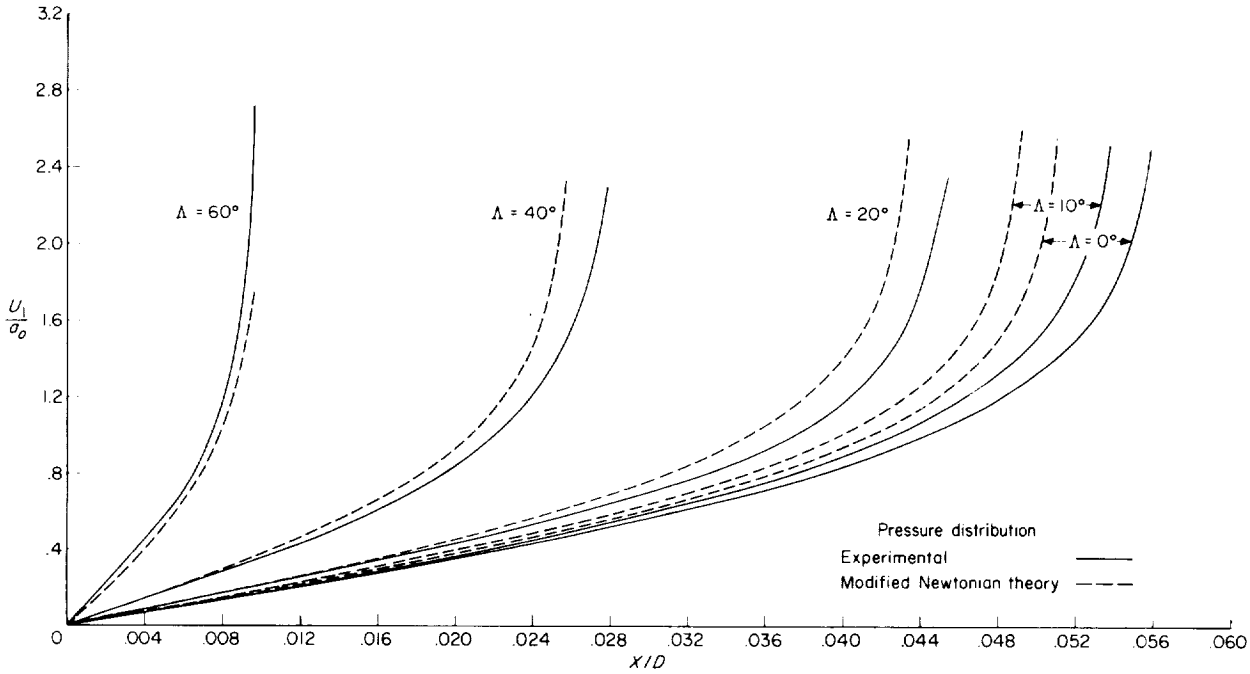

FIGURE 13. The variation of transformed chordwise velocity with transformed chordwise coordinate according to experimental and Newtonian pressure distribution

from the leading edge of the equivalent wedge flow. A sample calculation carried out by this procedure resulted in a heat-transfer coefficient about 7 percent less at $\theta^*=50°$ and $\Lambda=0°$ than the value obtained by using the first procedure. The method of reference 26 also resulted in larger values of β, namely, $\beta=2.00$ at $\theta^*=51.5°$ compared with $\beta=1.38$ obtained by using the method of reference 25. Since $\beta=2$ is the maximum value (from eq. (B11)) in the similar solutions, the method of reference 26 could not be used for $\theta^*>51.5°$ in this particular example.

REFERENCES

1. Feller, William V.: Investigation of Equilibrium Temperatures and Average Laminar Heat-Transfer Coefficients for the Front Half of Swept Circular Cylinders at a Mach Number of 6.9. NACA RM L55F08a, 1955.
2. Cunningham, Bernard E., and Kraus, Samuel: Experimental Investigation of the Effect of Yaw on Rates of Heat Transfer to Transverse Circular Cylinders in a 6500-Foot-Per-Second Hypersonic Air Stream. NACA RM A58E19, 1958.
3. Swanson, Andrew G.: Free-Flight Investigation of Aerodynamic Heat Transfer to a Simulated Glide-Rocket Shape at Mach Numbers up to 10. NACA RM L58G03, 1958.
4. Geodwin, Glen, Creager, Marcus O., and Winkler, Ernest L.: Investigation of Local Heat-Transfer and Pressure Drag Characteristics of a Yawed Circular Cylinder at Supersonic Speeds. NACA RM A55H31, 1956.
5. Beckwith, Ivan E.: Theoretical Investigation of Laminar Heat Transfer on Yawed Infinite Cylinders in Supersonic Flow and a Comparison With Experimental Data. NACA RM L55F09, 1955.
6. Reshotko, Eli, and Beckwith, Ivan E.: Compressible Laminar Boundary Layer Over a Yawed Infinite Cylinder With Heat Transfer and Arbitrary Prandtl Number. NACA Rep. 1379, 1958. (Supersedes NACA TN 3986.)
7. Beckwith, Ivan E., and Gallagher, James J.: Experimental Investigation of the Effect of Boundary-Layer Transition on the Average Heat Transfer to a Yawed Cylinder in Supersonic Flow. NACA RM L56E09, 1956.
8. Feller, William V.: Heat Transfer to Bodies at Angles of Attack. NACA RM L57D19e, 1957.
9. Reshotko, Eli: Laminar Boundary Layer With Heat Transfer on a Cone at Angle of Attack in a Supersonic Stream. NACA TN 4152, 1957.
10. Beckwith, Ivan E.: Similar Solutions for the Compressible Boundary Layer on a Yawed Cylinder With Transpiration Cooling. NASA TR R-42, 1959. (Supersedes NACA TN 4345.)
11. Stewartson, K.: Correlated Incompressible and Compressible Boundary Layers. Proc. Roy. Soc. (London), ser. A, vol. 200, no. A1060, Dec. 22, 1949, pp. 84–100.
12. Beckwith, Ivan E., and Gallagher, James J.: Heat Transfer and Recovery Temperatures on a Sphere With Laminar, Transitional, and Turbulent Boundary Layers at Mach Numbers of 2.00 and 4.15. NACA TN 4125, 1957.
13. Penland, Jim A.: Aerodynamic Characteristics of a Circular Cylinder at Mach Number 6.86 and Angles of Attack up to 90°. NACA TN 3861, 1957. (Supersedes NACA RM L54A14.)
14. Gowen, Forrest E., and Perkins, Edward W.: Drag of Circular Cylinders for a Wide Range of Reynolds Numbers and Mach Numbers. NACA TN 2960, 1953. (Supersedes NACA RM A52C20.)
15. Gregory, N., Stuart, J. T., and Walker, W. S.: On the Stability of Three-Dimensional Boundary Layers With Application to the Flow Due to a Rotating Disk. Phil. Trans. Roy. Soc. (London), ser. A, vol. 248, no. 943, July 14, 1955, pp. 155–199.
16. Seiff, Alvin: The Prospects for Laminar Flow on Hypersonic Airplanes. NACA RM A58D25, 1958.
17. Reynolds, W. C., Kays, W. M., and Kline, S. J.: Heat Transfer in the Turbulent Incompressible Boundary Layer. III - Arbitrary Wall Temperature and Heat Flux. NASA MEMO 12-3-58W, 1958.
18. Mager, Artur: Transformation of the Compressible Turbulent Boundary Layer. Jour. Aero. Sci., vol. 25, no. 5, May 1958, pp. 305-311.
19. Cohen, Nathaniel B.: A Method for Computing Turbulent Heat Transfer in the Presence of a Streamwise Pressure Gradient for Bodies in High-Speed Flow. NASA MEMO 1-2-59L, 1959.
20. Sommer, Simon C., and Short, Barbara J.: Free-Flight Measurements of Turbulent-Boundary-Layer Skin Friction in the Presence of Severe Aerodynamic Heating at Mach Numbers From 2.8 to 7.0. NACA TN 3391, 1955.
21. Turcotte, Donald Lawson: On Incompressible Turbulent Boundary Layer Theory Applied to Infinite Yawed Bodies. Graduate School Aero. Eng., Cornell Univ. (Contract AF 33 (038)-21406), Sept. 1955.
22. Young, A. D., and Booth, T. B.: The Profile Drag of Yawed Wings of Infinite Span. Aero. Quarterly, vol. III, pt. III, Nov. 1951, pp. 211–229.
23. Ashkenas, Harry, and Riddell, Frederick R.: Investigation of the Turbulent Boundary Layer on a Yawed Flat Plate. NACA TN 3383, 1955.
24. Colburn, Allan P.: A Method of Correlating Forced Convection Heat Transfer Data and a Comparison With Fluid Friction. Trans. Am. Inst. Chem. Eng., vol. XXIX, 1933, pp. 174–210.
25. Stine, Howard A., and Wanlass, Kent: Theoretical and Experimental Investigation of Aerodynamic-Heating and Isothermal Heat-Transfer Parameters on a Hemispherical Nose With Laminar Boundary Layer at Supersonic Mach Numbers. NACA TN 3344, 1954.
26. Smith, A. M. O.: Rapid Laminar Boundary-Layer Calculations by Piecewise Application of Similar Solutions. Jour. Aero. Sci., vol. 23, no. 10, Oct. 1956, pp. 901–912.

U.S. GOVERNMENT PRINTING OFFICE: 1962